CHAPTER 1- INTRODUCTION

1.1 General

Inverted-V-braced frame is a common type of concentrically braced frame generally called as chevron-braced frame (CBF). CBF in chevron configuration is a cost-effective system for resisting lateral loads. This structural system is usually employed for low-rise and mid-rise steel framed buildings. Braces in chevron configuration provide support for the CBF beams at the brace to beam intersection point [1-4].

The seismic behavior of such system is controlled by the buckling of the lower storey braces in compression (Figure 1.1). However, this system has not performed well and does not show much force redistribution capacity under strong earthquakes [1, 2].

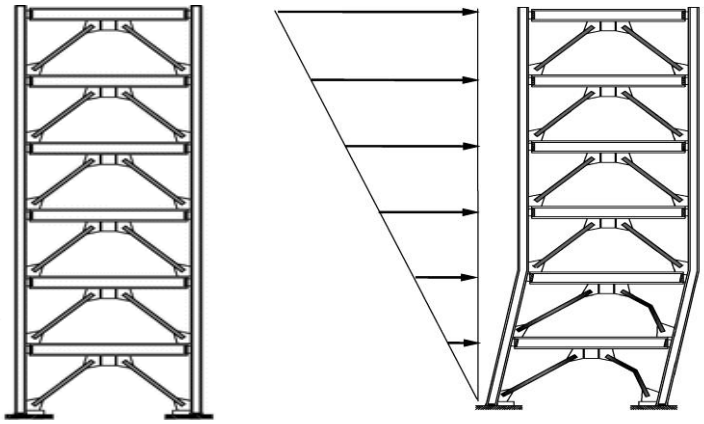

Figure 1.1: Buckling of CBF under lateral load

In strong seismic excitations, this configuration exhibits a concentration of damage within a single floor. For example, extensive damages were found in CBF buildings during Loma Prieta earthquake (1989), Northridge earthquake (1994), Kobe earthquake (1995), Christ church earthquake (2010), Tohoku earthquake (2011) and other events. In light of this, frequent damages were observed in braced frames where braces were proportioned to resist tension only, where connections were weaker than the braces attached to them,

where braces framed directly into columns, and where braces were inclined principally in one direction. Under strong ground motions, braces in compression have buckled, and in consequence lose their buckling resistance strength [3].

After buckling of braces occurred due to compressive force, due to the difference between the tensile and post-buckling capacity of brace members the unbalanced force developed at the braces to beam intersection point. Thereby, beams were deflected downward as a result of the combined action of this force and the gravity loading. These phenomenon demand strong floor beams to stabilize the system when the unbalance vertical load transferred from braces to beams has increased due to the attaining of the post-buckling strength in the compressive brace. As a result of this behavioral characteristic, with the increase of the building height, the CBF system shows a limited efficiency in terms of distributing the lateral loads.

This drawback pointed out by Khatib et al. [4]. Typically, in the CBF structures, excessive storey drifts is concentrated within a few stories and large ductility demand is required.

To overcome this, in the last two decades more emphasis has been placed to increase both the ductility and the energy dissipation capabilities of structures in seismic areas. It results development of design provisions for a new type of braced frame, called a special concentrically braced frame. Within these provisions, the performance of special inverted-V braced frames was improved compared with that of ordinary inverted-V-braced frames [5, 6]. However, special concentrically braced frames continue to exhibit a typical braced-frame design problem. With continued lateral displacement, the compression brace buckles and its axial load capacity decreases, whereas the tension brace force continues to increase until it reaches a yield statement. This creates a large, unbalanced vertical force on the intersecting beam. To prevent deterioration of the lateral strength of the frame, current design provisions require that the beam to have adequate strength to resist the

potentially significant post-buckling force in combination with appropriate gravity loads, resulting in very strong beams [7].

To address this adverse effect of the unbalanced force, Khatib et al [4] proposed a modified CBF system labeled CBF with zipper columns between brace-to-beam intersection points, as shown in Figure 1.2.

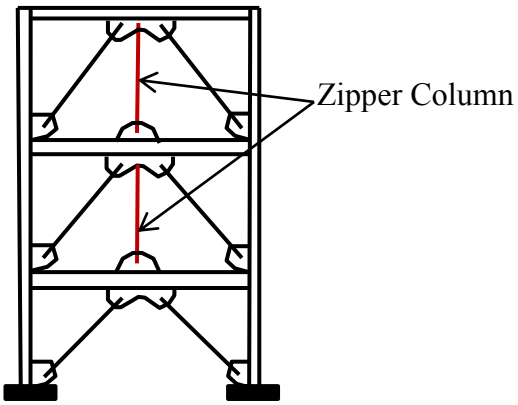

Figure 1.2: Integration of zipper column in CBF

In this bracing system, the unbalanced force, transmitted through the zipper element, increases the compression force applied to the upper story compression brace, eventually causing it to buckle. Here, concurrent buckling of braces over the height of a building will result in a more uniform distribution of damage as desired by the designer. However, instability and overall collapse can occur once the full-height zipper mechanism forms [7]. This disadvantage was overcome by introducing a suspension system, called a "suspended zipper-braced frame," (SZBF) as shown in Figure1.3.

In a SZBF, the top story bracing members are designed as larger one to remain elastic while all other compression braces have buckled and the zipper elements have yielded. Because the primary function of the suspended zipper struts is to sustain tension forces and the suspended zipper struts support the beams at the midspan, the beams can be designed to be flexible. This results in significant savings in material and cost in

suspended zipper frames. Moreover, the force path is so evident that a capacity design for all structural members is straightforward [2].

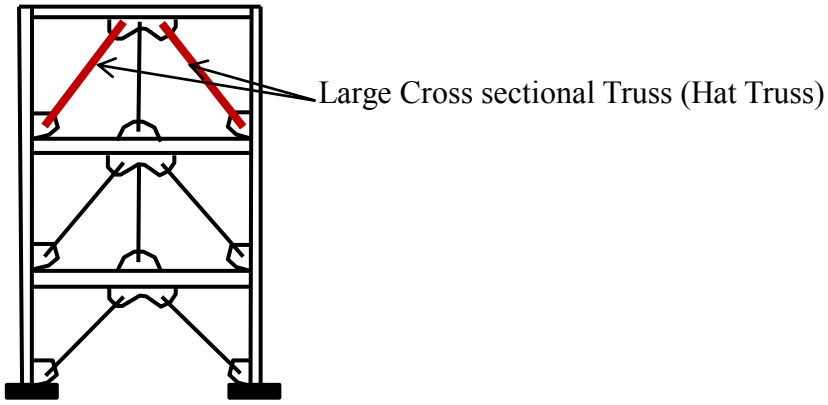

Figure 1.3: Large cross section of braces of top floor in SZBF

Yang et al. [1] performed an experimental pushover test on a one third-scale model of a SZBF. In their study, the zipper elements demonstrated their ability to activate buckling in all stories except the top one by redistributing the loads in the structure and minimizing strength losses [1, 8]. Chen refined the existing design method for CBF with strong zipper columns and validated the refined design method by studying the performance of CBF systems with strong zipper columns for low, mid and high-rise buildings [3]. However, in the experiments it is found that, as zipper elements of stories transfer unbalanced vertical forces of the lower stories to the upper ones, the tensile forces generated in these elements extremely increase in upper stories. Accordingly these zipper elements need an impractically large cross-section especially in tall buildings. Moreover, along with the increase in building height and stories number, undesired effects, such as excessive lateral deformation due to the activation of higher modes could drive the building near collapse.

In order to improve the seismic performance of a structure, numerous techniques have been widely used over the last few decades. The incorporation of innovative materials in bracing systems has been a widely accepted approach. In recent years, the structural engineering community has shifted its focus to the utilization of smart materials i.e. super-

elastic shape memory alloy (SMA) as a new component of structural systems to improve the performance of structures. Regular steel frames have been used in earthquake-vulnerable zones due to their ductile behaviour, but brittle fractures of the beam-column connections, brace-to-column and brace to beam connections have led researchers to incorporate special metals and/or smart material as bracing elements. These innovative materials exhibit interesting characteristics which have made them useful in improving the performance of structures [9, 10].

Nitinol is a type of smart material consists of Ni-Ti(Ni-Ti SMAs). These SMAs are unique materials which have the ability to undergo large plastic deformation under extreme loading conditions and return to their original shape upon the removal of the load. An SMA can recover a strain of about 10% without any permanent deformations. It is also highly resistant to corrosion. This unique and super-elastic (SE) characteristic of SMA makes it a potential candidate in regions with high seismic activity. However, the cost is much higher than the costs of regular steels. Still, SMA as a bracing agent has emerged as a suitable candidate over other materials due to its large deformability during earthquakes and recoverable capability after the earthquake. SMAs have an excellent re-centering capacity and energy absorbing capacity which reduce the vulnerability of the structure. This characteristic of SMAs improves the seismic performance of the given structure. Researchers are using SMA as a base-isolation; as a passive energy dissipation device; for the retrofitting of structures; and as a bracing element [11-13].

Hence, in this study, SMA frame was proposed to be used in brace elements instead of only conventional steel in a SZBF and then the seismic behavior of these frames was evaluated and compared between them. For this purpose, a pushover and incremental dynamic analysis were performed on SZBF (steel and SMA braced) of low and mid- rise (3 and 9 storied respectively) buildings and compared with that of equivalent CBF frames.

1.2 Objectives

The objectives of this study are:

- To investigate the seismic performance evaluation of steel and SMA based SZBF and steel CBF in terms of roof drift and inter-storey drift distribution of low and mid-rise steel building under static and dynamic loads using the freely available FE software, Seismostruct [14] .
- To improve understanding of the performance-based design components in seismic resisting structural systems.

1.3 Methodology

In order to achieve the above objectives, the following methodology is proposed:

1.3.1 2D steel frames of one bay of 3 storey (low rise) and 9 storey (mid-rise) steel building have been taken as reference models which were developed as suspended zipper braced frames through complementary experimental and numerical simulation approaches by Yang et. al. [1]. These structural systems were illustrated in his experiments with 3 and 9-story buildings designed for the same masses as those used in the SAC studies for the Los Angeles. In addition, equivalent CBF as designed by Ozcelik et. al. [15] has been taken for comparison purpose of CBF and SZBF.

1.3.2 To evaluate the performance of integrating SMA bracing system in SZBF, SMA has been added in place of inverted V steel braces following the design consideration of Asgarian [12]. All the computational models of the structure were developed using the modeling capability of the software framework of Seismostruct.

1.3.3 For performance evaluation of all the frames, pushover analysis and incremental dynamic analyses were involved by employing the Seismostruct software.

1.4 Thesis Organization

This thesis is organized in six chapters:

- The first chapter presents the introduction of research generalities, objectives, methodology, and thesis organization.
- The second chapter summarizes the literature review on the past studies conducted on zipper frame structure and use of SMA in steel frames.
- The third chapter contains the numerical modeling of reference models, there modifications according to the proposed design integrating SMA in bracing system and validation of numerical modeling with experimental results.
- The fourth chapter contains nonlinear static pushover analysis of all the models including determining the ductility, over strength factor and response modification factor.
- The fifth chapter highlights the selection of ground motion ensembles, the scaling process of the selected ground motions, and the seismic response of the 3 (low rise) and 9 storey (mid-rise) CBF, SZBF of steel and SMA under incremental dynamic analysis by Seismostruct and development of fragility curves from the probabilistic seismic demand models.
- Finally, in the sixth chapter, conclusions and the recommendations of the future works are presented.

CHAPTER -2: LITERATURE REVIEW

2.1 The Evolution of Suspended Zipper Braced Frame

To withstand earthquake loads, inverted V braced i.e. CBF is able to provide high stiffness and moderate ductility by allowing the braces to buckle and/or yield in order to dissipate the input energy during ground motion excitations, while all other structural members such as: beams, columns, and connections behave in elastic range. However, under strong seismic excitation, this system is prone to storey mechanisms, especially when beams are not designed to carry the unbalanced vertical load caused by buckled braces. (Figure 2.1) [1, 4]

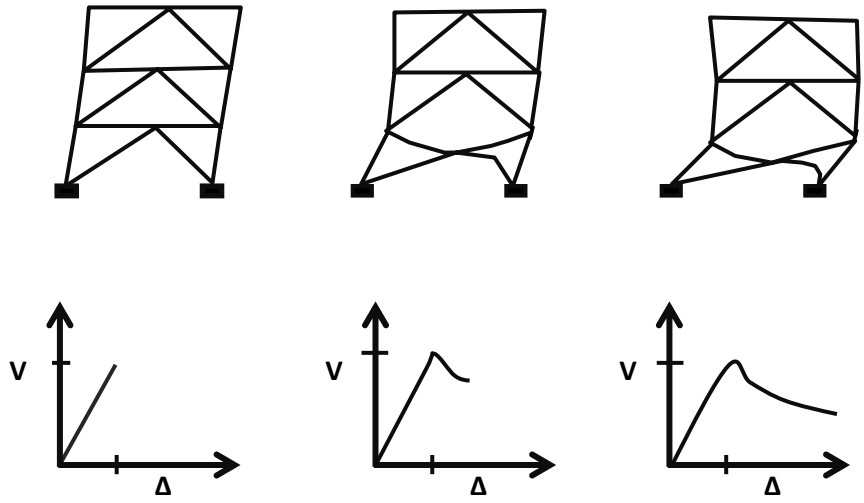

Figure 2.1 Chevron braced frame configuration and its failure mechanism

Thus, either the ground floor and/or the upper floors are prone to excessive lateral deformation after braces buckle and/or yield. Consequently, the sudden formation of the weak storey or storey mechanism drives the structure to failure instead of transferring the lateral forces to adjacent stories [1,2,4].

To overcome the problems caused by beam failure, several studies have been conducted by researchers, and the concept of strong beams, designed to carry the unbalanced forces developed when the braces lose their capacity in compression, was proposed. Despite this design strategy, the braced frame system is still prone to storey mechanism formation.

However, in solution of this, Khatib et al. [4] proposed to link all beam-to-brace intersection points of adjacent floor and to transfer the unbalanced load to the vertical element called zipper struts [1,3,16]. In "Zipper" configuration, the vertical braces transfer the unbalance force developed after the buckling of braces occurs in adjacent stories, and force the braces on these stories to buckle.

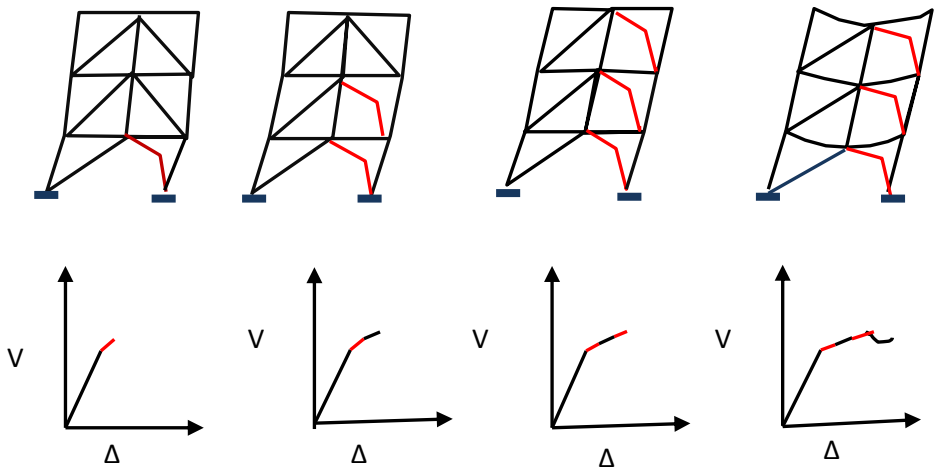

Figure 2.2 Expected behavior and performance of zipper frame [4]

Khatib investigated CBF systems with a variety of bracing configuration. For zipper braced frames, it was anticipated that the response would not be sensitive to ground motion signatures and it has a more uniform distribution of damage along the building height. Also, the story shear force-displacement curve is trilinear (Figure 2.2).

Later on, Sabelli [17] proposed design criteria for CBF with weak zipper strut. In this design method, zipper columns are allowed to buckle and to yield, while braces behave in inelastic range. He carried out study with 3 and a 6 storey zipper braced frames, and concluded that the inelastic demand on the braces is more uniformly distributed than in a chevron braced frame with strong beams. However, while the 3 storey zipper frame shows an outstanding behaviour under the ground excitations, and deflects based on the first mode shape, several behavioural aspects have been observed in the 6 storey frame. The deformed shape of the 6 storey frame approximates the shape of the second mode of vibration instead of the first mode, while significant buckling and tension yielding have been observed in the zipper columns.

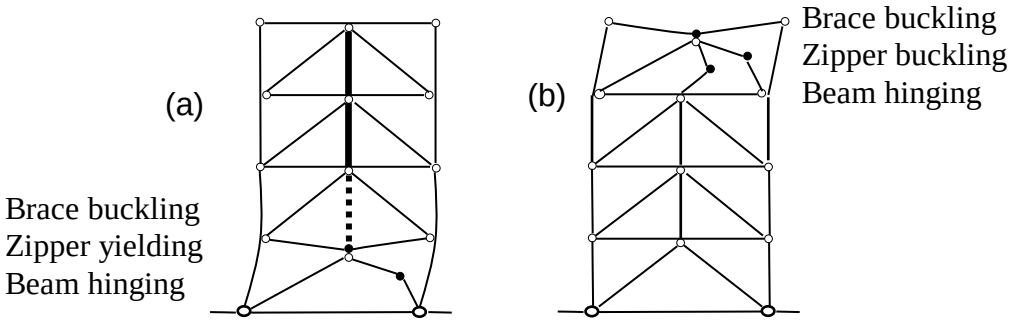

Figure 2.3 Behaviour of zipper braced frame system with weak zipper column:

(a) Zipper yields in tension; (b) Zipper buckles in compression [18, 19].

The behaviour of a chevron braced frame with weak zipper columns is shown in Figure 2.3. Both cases: zipper yielding and buckling are considered in design. With the aim of limiting the inelastic behaviour within braces, Tremblay and Tirca [18] have proposed a design method that relies on the ability of zippers to behave elastically. Based on their proposed design methodology, three zipper braced frame buildings (4, 8, and 12 storey) had been designed and investigated. Close examination of the inelastic behaviour of the aforementioned braced frames showed that both critical scenarios of zippers acting

in tension and compression can be treated separately. When the brace buckling initiates at the bottom storey and propagates upward in the frame, zipper columns are subjected to tensile forces due to the subsequent buckling of braces as shown in Figure 2.3 (a). On the other hand, when the first buckled brace is located at the top floor, as the buckling of braces propagates downward, the unbalance vertical forces, projected from the braces to mid-span of the beams, are transferred as compressive forces in zipper columns as shown in Figure 2.3(b).

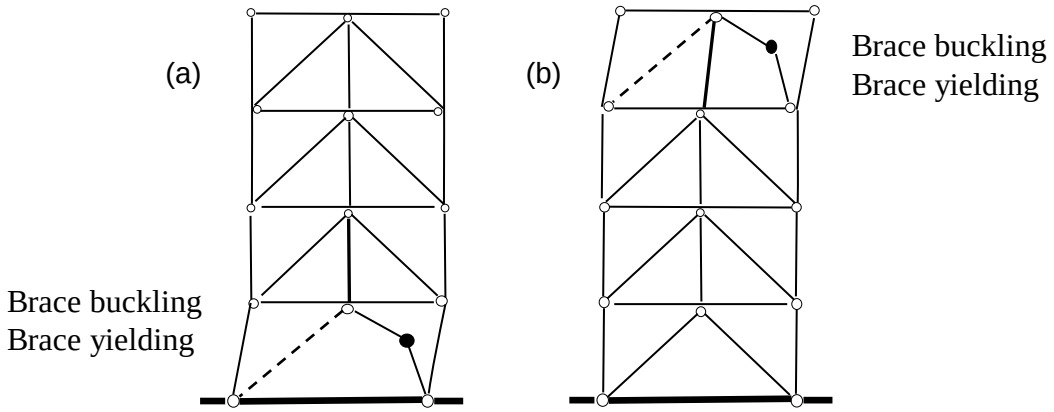

Figure 2.4 Behaviour of zipper braced frame system with strong zipper columns:
(a) Brace buckling initiated at the base, (b) Brace buckling initiated at the roof [18].

Therefore, the zipper columns are designed to carry the unbalanced load developed at the mid-span of the beams after braces buckle. To assess the force in zippers and their required compressive and tensile strength, the following two scenarios have been proposed: zippers act in tension when the first brace buckles at the base and zippers act in compression when the first brace buckles at the top of the structure (Figure 2.4).The zipper struts are designed to withstand both of the maximum compressive force and the maximum tensile force which would be induced by the internal forces which are equal to the probable buckling/post buckling capacity and the tensile capacity of braces.

Roberto Lean and Young [21] proposed a modified zipper braced frame called suspended zipper frame. This system consists of a zipper frame system with a hat truss (an increased size brace) located at the top floor level. This concept requires the top storey braces to remain elastic and prevent the full zipper mechanism formation. The suspended zipper frame consists of a partial height zipper braced frame and an elastic hat truss at the top floor with the aim to prevent the overall collapse of the structure (Figure 2.5). The suspended zipper columns are able to transfer the unbalanced vertical forces developed gradually due to the brace's inelastic behaviour at the lower part of the structure to the top storey braces and support the beams at mid-span. As a result, the beams can be design to hinge, which means reduced beam sizes and a more economical design.

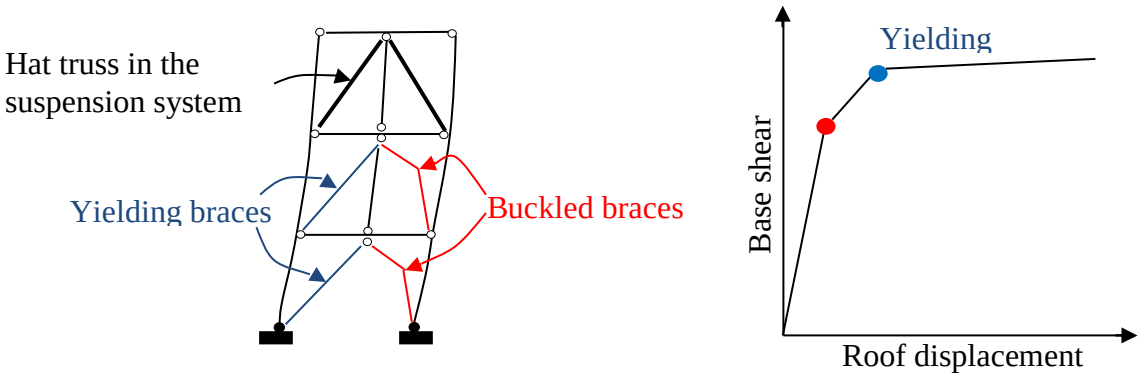

Figure 2.5 Suspended zipper column design and its push-over curves

In this method, the top level braces remain in elastic range while all other compression braces in other stories have buckled. In this frame, the top floor bracing members are designed to be bigger than the lower floor ones so as to suspend the zipper struts from the roof of the structure. Accordingly, the suspended zipper struts undergo the unbalanced vertical forces induced by lower floor bracing members in combination with gravity loads collected from the beams when the structures enter the nonlinear range.

2.2 Use of SMA in Braced Frame and SZBF

So far no literature has been found regarding the integration of SMA in SZBF. However several experiments have been done to find out the behavior of steel braced frames integrated with SMA braces [9-11, 21-24].

Asgarian et. al. [12] investigated the seismic performance of steel frames equipped with super elastic SMA braces. They considered buildings with various stories and different bracing configurations (diagonal, split X, chevron) for their experiment and concluded that in earthquake excitations use of SMA element is an effective way to improve the dynamic response of structures.

Jason et. al. [21] studied three- and six-story concentrically braced frames with superelastic shape memory alloy (SMA) braces to evaluate their seismic performance in comparison to traditional systems. Their results suggest that the SMA braces, due to the recentering nature, are effective in limiting interstory drifts and residual drifts during an earthquake.

Moradi et. al.[22] examined the seismic performance of four-storey concentrically braced frames (with four different bracing configurations; diagonal, split-X, chevron-V and inverted-V) equipped with either steel buckling-restrained braces or buckling-restrained SMA braces through incremental dynamic analysis. The results show that the SMA braces lead to a uniform distribution of inelastic response over the height of the building. It also mitigates seismic response in terms of maximum inter-storey drift and residual roof displacement. Moreover from the result, it is found that the SMA braces can be more beneficial especially under severe ground motion excitations.

CHAPTER 3- DEVELOPMENT OF STRUCTURAL SYSTEMS AND NONLINEAR MODELS

3.1 Design Approach

After the Northridge and Kobe earthquakes, SAC was formed by the joint venture of SEAoC (Structural Engineers Association of California), ATC (Applied Technology Council), and CUREE (California Universities for Research in Earthquake Engineering) that studies steel connections and structural systems. Various theme structures designed by SAC are commonly used as references for assessing performance of new or improved structural systems.

For the analytical experiment, two SZBF of 3 and 9 story buildings designed by Yang et al [1] has been taken in this study. These two zipper braced frames were designed to carry the same masses and use the same number of seismic-resisting bays as the 3 and 9-story SAC moment-resisting frames designed for downtown Los Angeles. To compare the seismic performance between SMA and steel bracing of SZBF, bracing materials of these two frames has been replaced by SMA. Moreover, two equivalent CBF frame as designed by Ozcelik et al [15] have also been analysed under static and dynamic loads to provide a detail comparison of all these systems.

In the Los Angeles area for the 2 % probability of exceedance in 50 years, the mapped spectral accelerations for the short period (S_s) and the 1 sec (S_1) period are 2.16g and 0.72g respectively, with a PGA of 0.90 g. The lateral load was designed from Chapter 12 of ASCE 7-05 [1]. For the building design, soil condition was considered as stiff soil (site class D as per ASCE 7-05 definitions), importance factor of 1.5 was assigned to the buildings in accordance of Occupancy Category IV. This is a significant departure from

the SAC building which was intended to determine whether zipper frames could be applicable even to critical structures. The response modification coefficient R was taken as 6, which is consistent with other ductile braced systems like special steel concentrically braced frames [1].

The floor plans and elevations for the buildings were predetermined, as shown in Figure 3.1. The location of the zipper-braced frames is shown by the bold lines in figures, and took up the same number of bays as for the special moment frames in the original SAC designs.

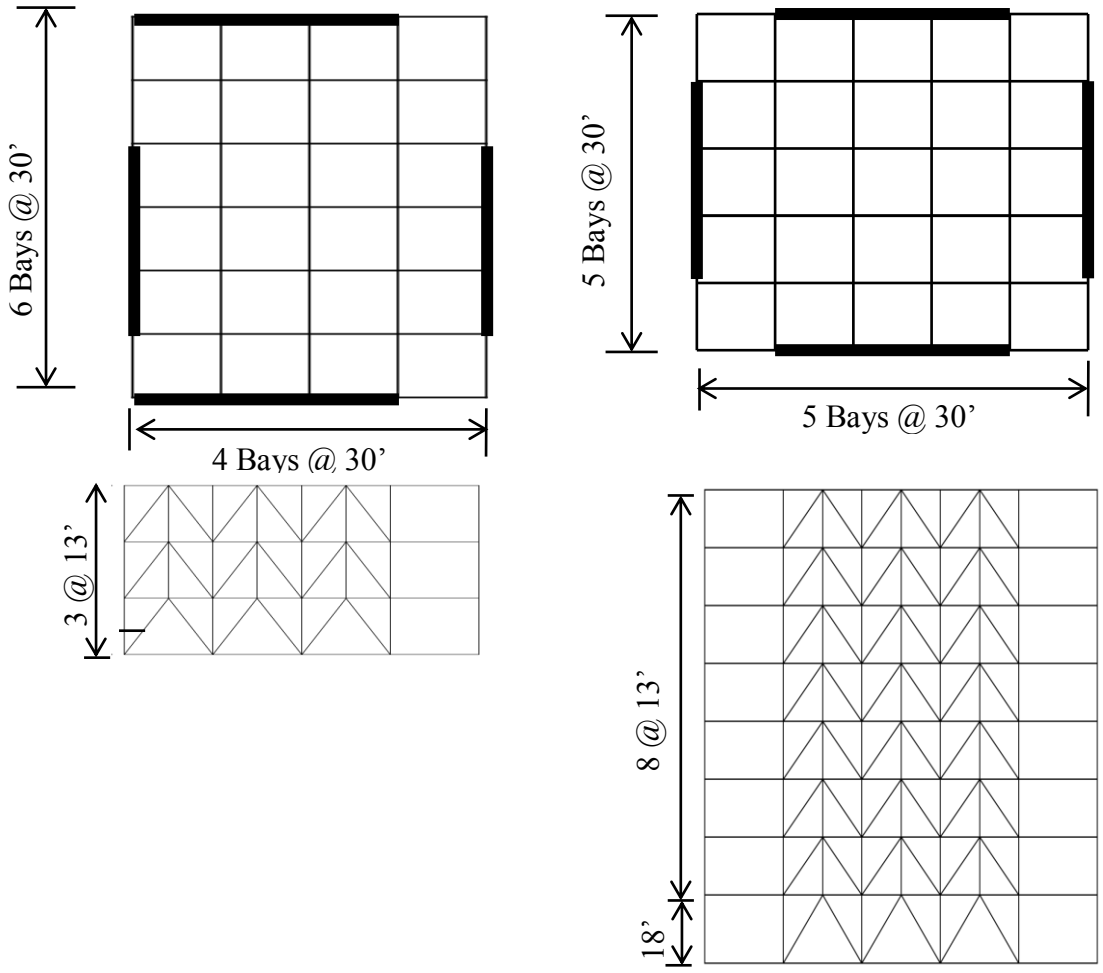

Figure 3.1: Floor Plan and Elevation of Model Buildings [1]

For the analysis of the buildings following floor load distribution (assuming steel weight as 13 psf for all designs) has been used:

- Floor dead load for weight calculation: 96 psf (4600 Pa)
- Roof dead load: 83 psf (3975 Pa)
- Reduced live load (floor and roof): 20 psf (900 Pa)

The models described above were used to investigate the zipper-braced models of 3-story bay and 9-story bay. The members selected for the 3 and 9 story zipper-braced bays are shown in Tables 3.1 and 3.2 respectively. The elevations of the two one bay frame models are also shown in Figure 3.2.

Table 3.1: Member sizes for the 3 storey zipper braced bay

Storey	Brace	Column	Beam	Zipper Strut
3	W14 x 132	W12 x 96	W8 x 58	W12 x 96
2	HSS8 x 8 x 1/2	W12 x 96	W10 x 88	W12 x 45
1	HSS8 x 8 x 5/8	W12 x 96	W10 x 88	

Table 3.2: Member sizes for the 9 storey zipper braced bay

Storey	Brace	Column	Beam	Zipper Strut
9	W14 x 398	W14 x 257	W10 x 68	W14 x 398
8	HSS7 x 7 x 1/2	W14 x 257	W14 x 257	W14 x 370
7	HSS8 x 8 x 1/2	W14 x 257	W10 x 88	W14 x 342
6	HSS8 x 8 x 5/8	W14 x 283	W10 x 88	W14 x 283
5	HSS9 x 9 x 5/8	W14 x 283	W12 x 96	W14 x 233
4	HSS9 x 9 x 5/8	W14 x 311	W12 x 96	W14 x193
3	HSS10 x 10 x 5/8	W14 x 311	W12 x 96	W14 x 132
2	HSS10 x 10 x 5/8	W14 x 342	W12 x 96	W14 x 82
1	HSS12 x 12 x 5/8	W14 x 342	W12 x 96	

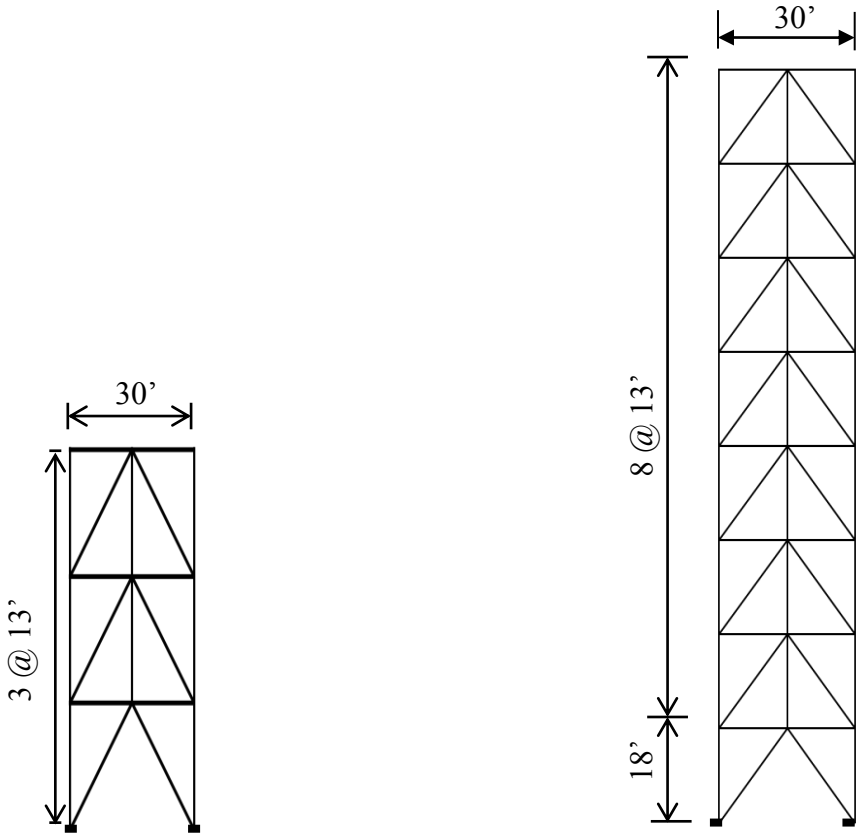

(a) (b)

Figure 3.2: Zipper braced model (a) 3 Storey Bay; (b) 9 Storey Bay

The member sizes of equivalent CBF frame which Ozcelik et al [15,25] redesigned removing the hat truss and zipper columns, and by providing storey beam design in accordance with AISC seismic provisions to carry out unbalanced vertical forces developing in the post buckling range has been listed in Tables 3.3 and 3.4.

Table 3.3: Member sizes for the 3 storey CBF

Storey	Brace	Column	Beam	Zipper Strut
3	HSS8 x 8 x 1/2	W12 x 96	W44 x262	-
2	HSS8 x 8 x 1/2	W12 x 96	W44 x262	-
1	HSS8 x 8 x 5/8	W12 x 96	W44 x290	

Table 3.4: Member sizes for the 9 storey CBF

Storey	Brace	Column	Beam	Zipper Strut
9	HSS7x 7 x 1/2	W14 x 257	W44x 230	-
8	HSS7 x 7 x 1/2	W14 x 257	W44x 230	-
7	HSS8 x 8 x 1/2	W14 x 257	W44x 262	-
6	HSS8 x 8 x 5/8	W14 x 283	W44x 290	-
5	HSS9 x 9 x 5/8	W14 x 283	W44x 335	-
4	HSS9 x 9 x 5/8	W14 x 311	W44x 335	-
3	HSS10 x 10 x 5/8	W14 x 311	W40x 392	-
2	HSS10 x 10 x 5/8	W14 x 342	W40x 392	-
1	HSS12 x 12 x 5/8	W14 x 342	W40x 431	

3.2 Numerical Modeling of the Braced Frames

The numerical models of the structure implemented in this study were developed using the nonlinear finite element based software "Seismostruct". Beam, column, bracing, zipper struts of the models were generated using the inelastic force-based (infrmFB) frame elements [14, 26, 27], which are capable of modelling members of space frames with geometric and material nonlinearities. Large displacements/rotations and large independent deformations relative to the frame element's chord (also known as P-Delta effects) are taken into account in Seismostruct, through the employment of a total co-rotational formulation developed and implemented by Correia and Virtuoso [28].

3.3 Material Modeling

3.3.1 Conventional Steel

To model the steel's behavior, 'Menegotto-Pinto steel model (stl_mp) an uniaxial steel model on a simple, yet efficient, stress-strain relationship proposed by Menegotto and Pinto [29] coupled with the isotropic hardening rules proposed by Filippou et al. [26] was

assigned to the elements in Seismostruct. Considering the idealized elastoplastic behavior of steel materials, compressive and tensional yield stresses (F_y= 345 MPa for column and beam, F_y= 317 MPa for bracing and zipper) used in Yang's experiments [1] were considered equal to steel's yield stress. The cross-section behaviour is reproduced by means of the fibre approach, assigning a uniaxial stress-strain relationship at each fibre. A number of 150 fibers were used to mesh the cross section of braces. The Menegotto-Pinto (MP) hysteretic model [29] was used to simulate the steel behavior. The material parameters are reported in Table 3.5, while the numerical response envelope is plot in Figure 3.3.

Table 3.5 Input parameters of steel hysteretic models in Seismostruct software

Steel Model	E_h	R_0	A_1	A_2	A_3	A_4
MP	0.025	20	18.50	0.15	0.00	1.00

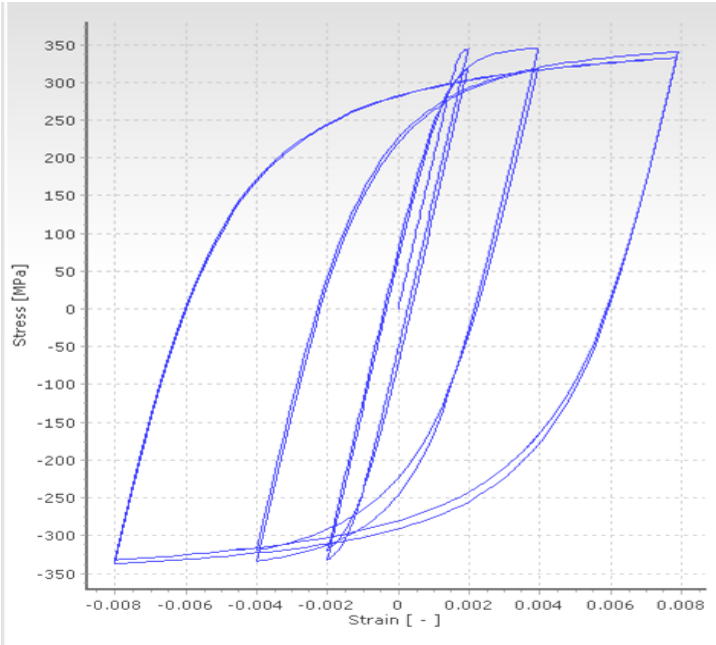

Figure 3.3: Menegotto-Pinto steel model (stl_mp) [29]

3.3.2 SMA

In the present study, SMA is incorporated as a bracing element. Therefore, one-dimensional model is perfect to fulfill the purpose of the material modelling. SMA bracing is modeled according to the model of Auricchio et al. [30]. Recently various researchers used this material modelling approach to model SMAs [9,10]. Figure 3.4 depict the typical stress-strain diagram of the SE-SMA, and the 1-D super elastic model used in the Seismostruct [14]. Table 3.6 shows material strength of SMA and steel used in this FE analysis.

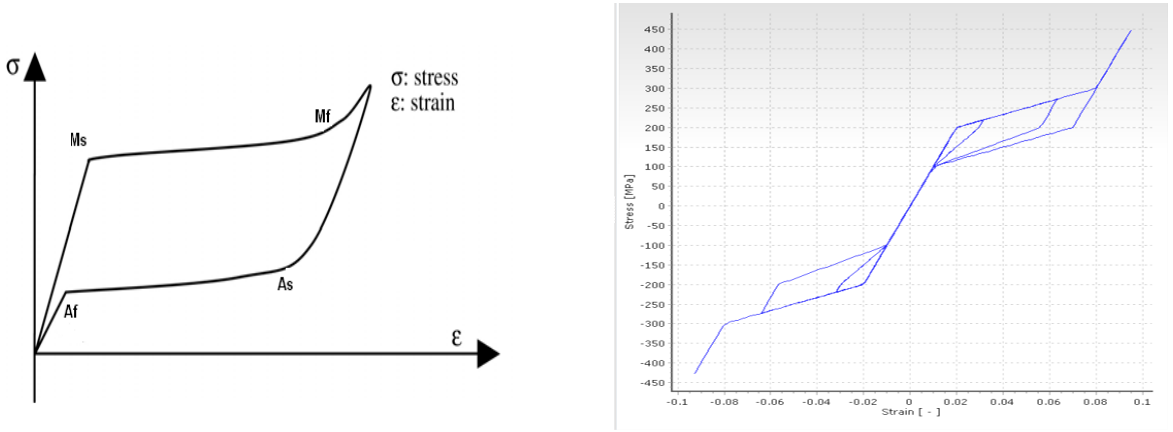

Figure.3.4. (a) Stress–strain relationship of the SMA, (b) Super elastic model of SMA

Table 3.6 Material properties used in the finite element analyses [1, 31].

Materials	Mechanical property	Value
Steel	Modulus of elasticity (GPa)	200
	Yield strength (MPa)	345
	Strain hardening parameter (%)	0.5
SMA	Modulus of elasticity (GPa)	27.58
	Austenite-to-martensite starting stress (MPa)	414
	Austenite-to-martensite finishing stress (MPa)	550
	Martensite-to-austenite starting stress (MPa)	390
	Martensite-to-austenite finishing stress (MPa)	200
	Superelastic plateau strain length (%)	5.0

3.4 Modeling of Frames

Link elements have been used in connection of all frame members, beam members has been designed as truss elements. Therefore, under gravity loads, beams will behave elastically and are not parts of the lateral resisting system. For the dynamic analysis, story masses were placed in the story levels considering uniform distributed load along the beam. A damping coefficient of 5% was assumed [1, 10, 12].

Following the Yang's model [1,15] a large initial mid span imperfection $L_w/150$ as shown in the Figure 3.5 perpendicular to the length for all braces was considered and a fiber cross section element was considered for plastification of the element over the member's length and cross section for linear and nonlinear buckling prediction. In the frame an additional joint was added at the middle length of a bracing member to obtain the imperfection. A fixed stiffness of rotational spring has also been used in the brace beam and brace column connection following the design implemented in Yang's experiment. Larger initial imperfection ratio for the braces were adopted to lower the maximum compression strength of the braces to get a more accurate simulation of the trilinear behavior, and two rotational springs were added at the end nodes of the brace to increase its maximum compression and minimum post-buckling strengths.

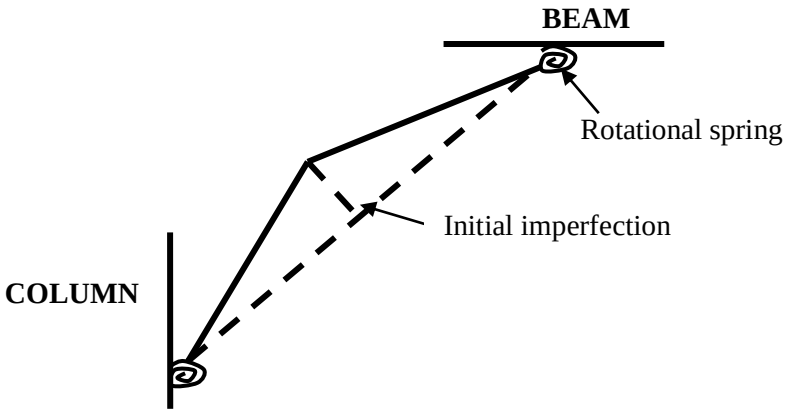

Figure 3.5: Initial imperfection of the braces perpendicular to its length

About designing of the SMA braces, cross section and length of the SMA elements are determined by following formula [32] and shown in Figure 3.6:

- $A^{SMA} = F_y/\alpha^{AS} = 317x\ A^{Steel}/414$ (3.1)

  $=0.77\ xA^{Steel}$

- $L^{SMA} = E^{SMA}A^{SMA}/K$ (3.2)

  $= E^{SMA}A^{SMA}L^{Steel}/\ E^{Steel}A^{Steel}$

  $= 27.579x0.77/2000 \times L^{Steel}$

  $= 0.107 \times L^{Steel}$.

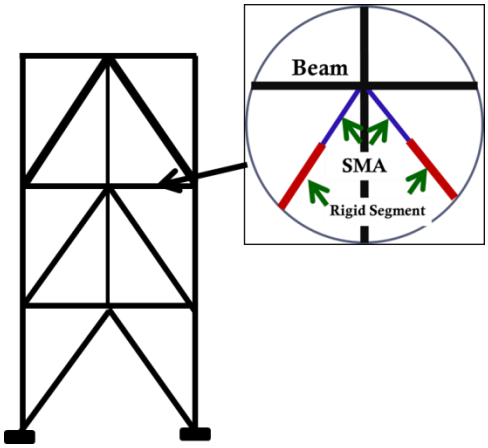

Figure 3.6: Length of SMA in bracing with rigid segment

3.5 Validation of Numerical Modeling with Experimental Result

3.5.1 Test Frame

Yang in his experiments prepared a test frame of 1/3 scale zipper braced frame model as shown in Figure 3.7 [1]. The member sizes of the frame have been given in Table 3.7.

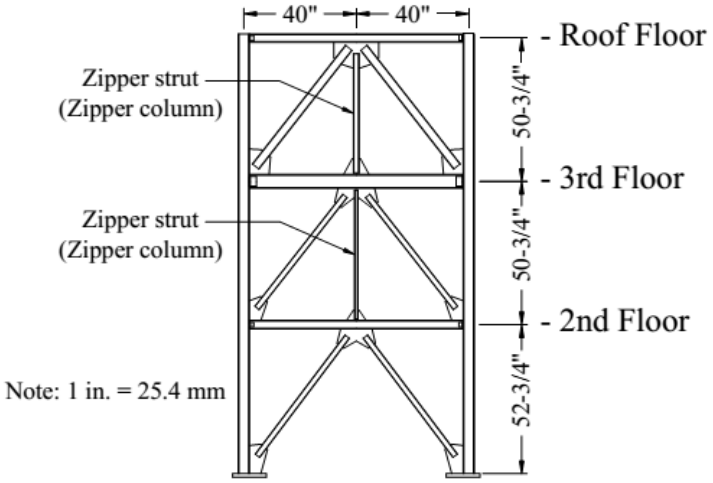

Figure 3.7 Elevation of the 1/3 scale test frame [1]

In this frame columns and beams were designed using A572 Grade 50 (F_y=345 MPa and F_u=448 MPa). The column base and gusset plates were made of ASTM A36 steel (F_y=250 MPa and F_u=400 MPa). The braces and the zipper struts in the zipper-braced frame model were hollow square section (HSS) made of ASTM A500 Grade B steel (F_y=317 MPa and F_u=400 MPa).

Table 3.7: Member sizes for the 1/3 scaled 3 storey zipper braced bay

Storey	Brace	Column	Beam	Zipper Strut
3	HSS3×3×3/16	S4×9.5	S3×5.7	HSS2×2×3/16
2	HSS2×2×1/8	S4×9.5	S5×10	HSS1.25×1.25×3/16
1	HSS2×2×1/8	S4×9.5	S3×7.5	

3.5.2 Loading

A set of three time histories of floor displacements as shown in Figure 3.8 were applied into three actuators at each floor levels of the test frame. Yang took these applied

displacements from the pre-experiment results of nonlinear static analyses of the reduced-scale model using OpenSEES [51].

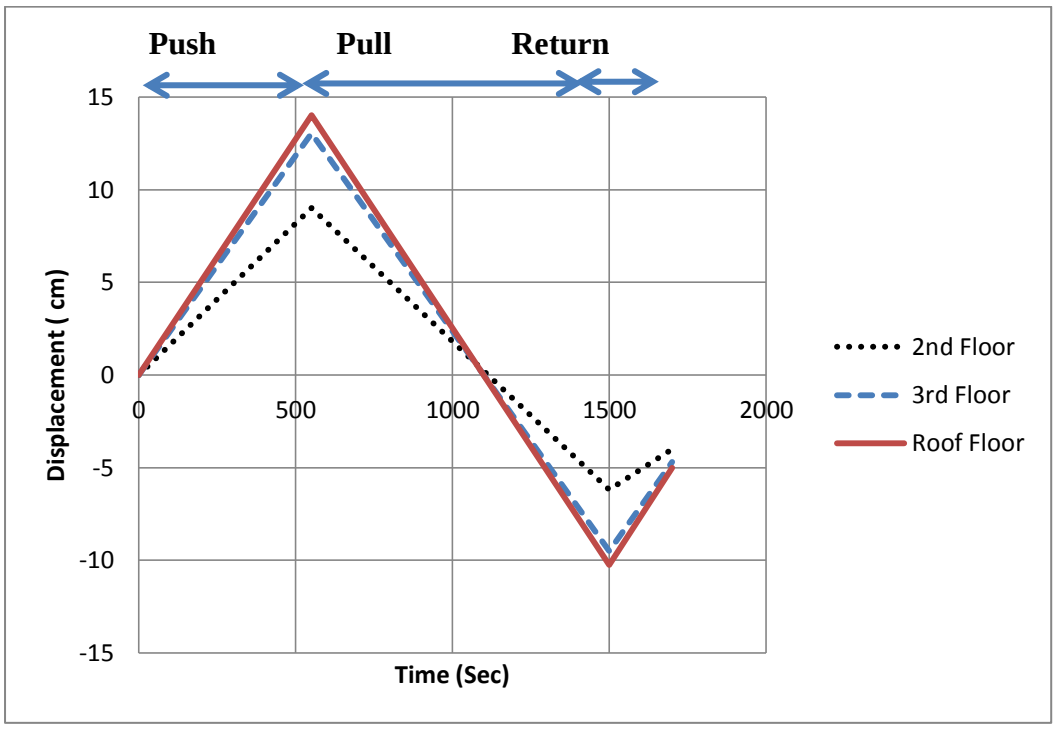

Figure 3.8: Applied displacement histories.

The frame was pushed southwards (let's say rightward) to a roof displacement of +14.02 cm (+5.52 in), then pulled northwards (leftwards) to -10.26 cm (-4.00 in), and returned to -5.08 cm (-2.00 in) where the base shear was close to zero. The maximum positive value, 14.02 cm, of the roof displacement was designated as the target displacement. This value was the largest among the maximum roof displacements from the results of 20 nonlinear dynamic analyses performed on the model.

In these analyses, three important assumptions were made:

- The damping ratios for the first and third modes were specified as 5% for constructing a Rayleigh damping spectrum.

- The second-floor and third-floor beam-to-column connections were modeled as rigid and the ends of both the braces and suspended zipper struts were assumed as partially restrained connections with a rotational stiffness of 113 m-kN/rad (as a weak spring).
- The initial imperfection ratio of the braces was assumed to be $L_w/2000$.

3.5.3 Numerical Simulation of Test Frame in Seismostruct

A similar 2D frame of 1/3 scale test frame (Figure 3.9) was developed in Seismostruct following the properties and assumptions of Yang's experiments [1]. Three time history curves (time-displacement) have been developed using the values obtained from graphs of Figure 3.8. A nonlinear static time history analysis has been carried out applying the loads in three floor levels and a hysteric curve of base shear vs. roof displacement was obtained from post processing output.

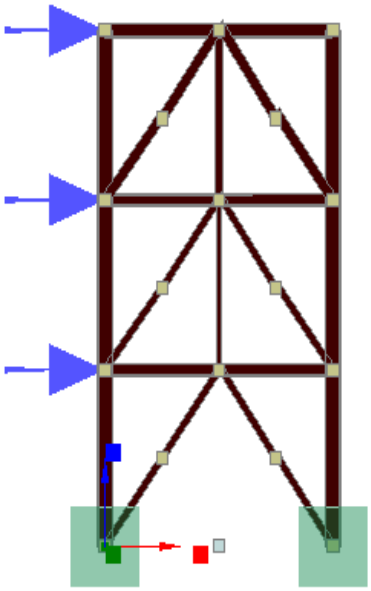

Figure 3.9: Seismostruct model similar to 1/3 scale Zipper Braced Frame

3.5.4 Test Output and Comparison of Graphs: Behavior of the Zipper-Braced Frame Models

As shown in Figure 3.10, a trilinear skeleton curve (experimental and simulated) approximately represents the hysteretic behavior up to the target roof displacement. The experimental graph has been taken from the Yang's experiment which was performed at the Structural Engineering Laboratory at Georgia Tech using the pushover testing method [1]. The summary of the test is tabulated at Table 3.8.

Table 3.8 : Corresponding Roof Displacement and Base Shear of Test Frame

Point	Roof Displacement (cm)	Base Shear (kN)	
		Experimental	Simulated
A	1.52	187	193
B	2.29	205	213
C	3.81	271	273
D	7.62	276	277
Target (R)	14.02	280	282
E	8.38	-76	-89
F	0	-156	-163
Fracture	-3.05	-102	-187
Target (L)	-10.26	-109	-216

In the graph of experimental one (Figure 3.10) the initial section corresponds to approximate linearly elastic behavior to Point A. At Point A, the first-story right brace buckled, followed shortly by buckling of the second story right brace at Point B. As a result, the subsequent structural stiffness decreased. As the zipper frame was pushed to Point C, both the right column base and the first-story left brace started to yield. The left column base yielded fully at a little beyond Point C, and the maximum lateral resistance of the zipper frame approached to 280 kN. At Point D, the second-story zipper strut yielded. Finally, when pushed to the target roof displacement, the zipper frame retained its maximum lateral-resistance capacity.

Once the initial target displacement was reached (i.e rightwards 14.02 cm), the zipper frame was unloaded and pulled back to the roof displacement -10.26 cm. When the zipper frame passed point E, the first-story left brace initially buckled at a load of about -89 kN which was smaller than the first buckling strength of -138 kN of the first-story right brace. As the displacement was reversed, the left brace carried most of the lateral load as it had yielded extensively in tension during the initial push cycle. The heavily buckled right brace contributed little to the lateral resistance. Upon further pulling to a roof displacement of 5.08 cm the second-story left brace also buckled at a load of about -124 kN. This was smaller than the buckling strength of -187 kN of the second-story right brace. As the original position of the roof was reached (Point F), a portion of the middle of the first-story right brace, which had experienced local severe buckling during the pushing test, began to tear due to large tension force developed in the brace. At a roof displacement of -3.05 cm, the torn section completely fractured, and the strength of the zipper frame decreased from -169 kN to -102 kN.

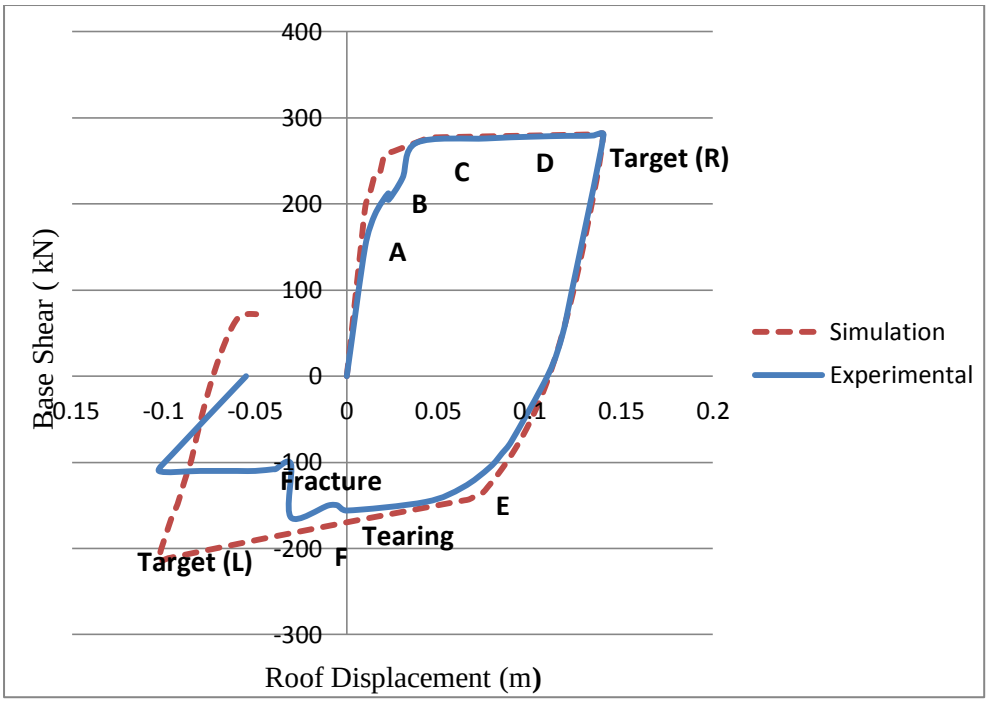

Figure 3.10: Hysteric response of the zipper braced frames

The simulated hysteric response graph of Figure 3.10 has been obtained from the static time history analysis of the similar 2D frame developed by Seismostruct software and applying the time history curves from Figure 3.8. Comparing the two graphs, in general, the simulation can predict behavior satisfactorily until a portion of the middle section in the brace starts to tear. This is because the Seismostruct element used in these studies cannot simulate the reduction in the cross-section area after the brace begins to tear. However, as initial buckling and yielding strength, the analytical results are in good agreement with the experimental data.

The analytical results confirmed the experimental observation that the initial buckling strength of a brace subjected to tension first is smaller than that of a brace subjected to compression first.

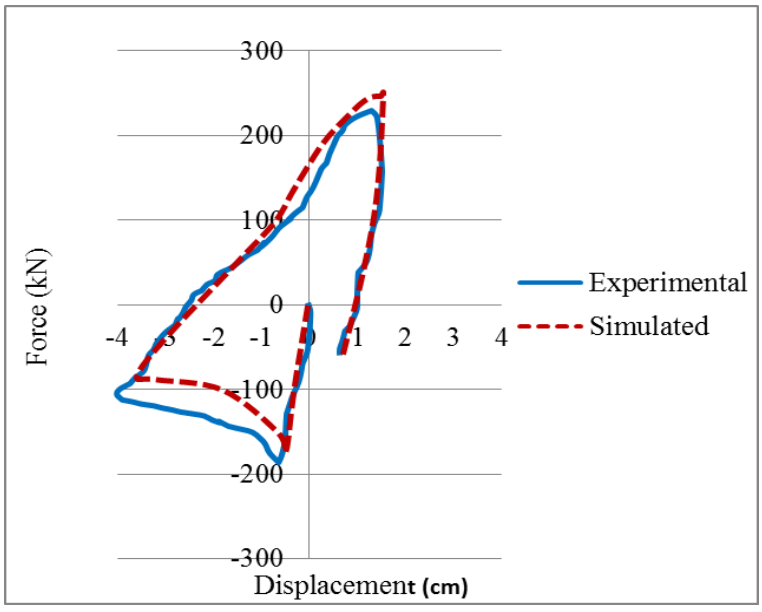

Figure 3.11: Hysteric curve of second storey right brace

In analyzing the force displacement graph of the braces, in the second story right brace, buckling occurred at an axial displacement of -0.51 cm which corresponds to a force of about -187 kN, as shown in Figure 3.11. When the frame reached the target roof displacement, the compression force in the right brace decreased to -125 kN. The

simulated hysteric curve obtained from numerical analysis also placed in the graph to compare the simulated and experimental values of the brace. In this case also, the analytical results are showing good agreement with the experimental data.

3.6 Conclusion

The reference models of 3 and 9 storey SZBF have been numerically modeled in Seismostruct using steel and SMA in bracings. The experimental results of the 1/3 scale test frame carried out by Yang et.al.[1] have been found in good agreement with the simulated results obtained from the software output and hence validated the compatibility of numerical modeling of the frames to carry out the analysis.

CHAPTER 4: NON LINEAR STATIC PUSHOVER ANALYSIS

4.1 Nonlinear Pushover Analysis

Pushover analysis is a performance-based methods required for reasonable estimates of inelastic deformation or damage in structures. Pushover analysis, in addition to providing estimates of deformation demands, provides some useful insight into the pattern of inelastic deformation that may occur [17].

This is very important when assessing desirable behaviors such as strong column weak-beam behavior. In pushover analysis an inelastic model is developed and is subjected to gravity load followed by a monotonically increasing static lateral load.

Although the use of the nonlinear static pushover came in to practice in 1970's the potential of the pushover analysis has been recognized for only last two decades. Pushover analysis is mainly used to estimate the strength and drift capacity of existing structure and the seismic demand for this structure subjected to selected earthquake. This procedure can be used for checking the adequacy of new structural design as well. The effectiveness of pushover analysis and its computational simplicity brought this procedure in to several seismic guidelines (ATC 40 and FEMA 356) and design codes (Eurocode 8 and PCM 3274) in last few years [33-36].

In pushover analysis, a mathematical model directly incorporating the nonlinear load-deformation characteristics of individual components and elements of the building shall be subjected to monotonically increasing lateral loads representing inertia forces in an earthquake until a 'target displacement' is exceeded (Figure 4.1). A pushover analysis consists of two parts. First, the pushover or "Capacity Curve" is determined through

application of incremental static loads to an inelastic model of the structure. Second, this curve is used with some other "Demand" tool to determine the target displacement.

Target displacement is the maximum displacement (elastic plus inelastic) of the building at roof expected under selected earthquake ground motion. Pushover analysis assesses the structural performance by estimating the force and deformation capacity and seismic demand using a nonlinear static analysis algorithm. The seismic demand parameters are global displacements (at roof or any other reference point), storey drifts, storey forces, and component deformation and component forces. The analysis accounts for geometrical nonlinearity, material inelasticity and the redistribution of internal forces.

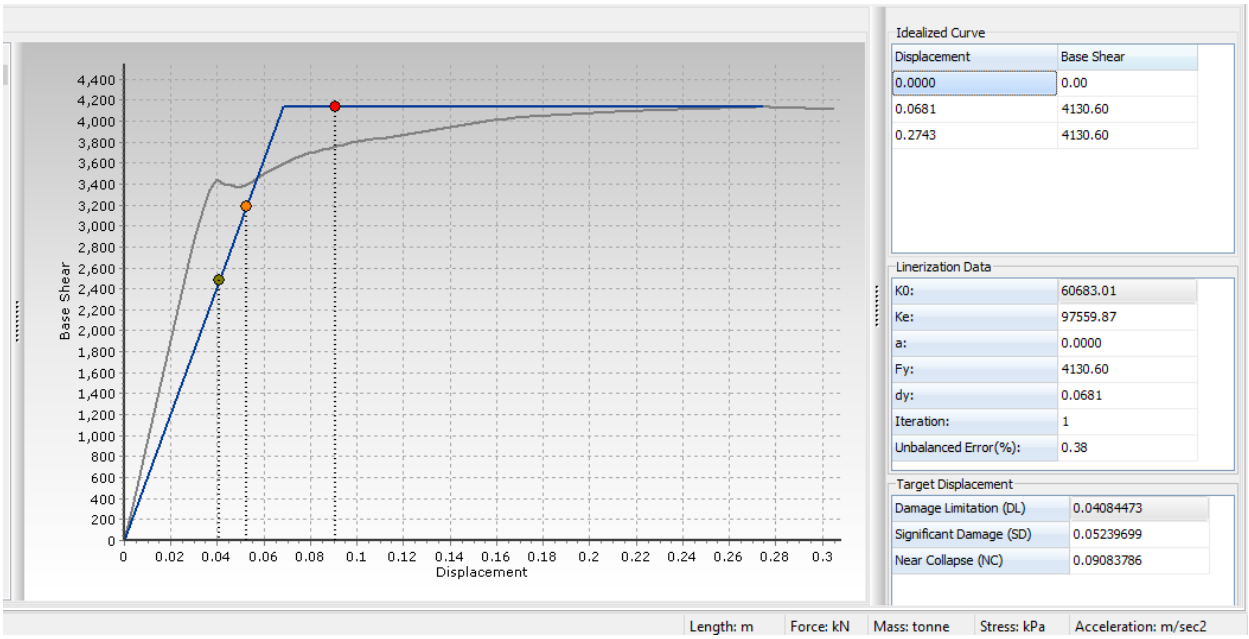

Figure 4.1: Pushover curve showing various target displacements

Response characteristics that can be obtained from the pushover analysis are summarized as follows [32]:

- Estimates of force and displacement capacities of the structure. Sequence of the member yielding and the progress of the overall capacity curve.

- Estimates of force (axial, shear and moment) demands on potentially brittle elements and deformation demands on ductile elements.
- Estimates of global displacement demand, corresponding inter-storey drifts and damages on structural and non-structural elements expected under the earthquake ground motion considered.
- Sequences of the failure of elements and the consequent effect on the overall structural stability.
- Identification of the critical regions, where the inelastic deformations are expected to be high and identification of strength irregularities (in plan or in elevation) of the building.

Pushover analysis delivers all these benefits for an additional computational effort (modeling nonlinearity and change in analysis algorithm) over the linear static analysis.

4.2 Lateral Load Profile

To evaluate the overstrength factor (R_o) and ductility (μ) of the SZBFs static nonlinear pushover analyses were carried out in 2D frame by using Seismostruct. Lateral loads were triangularly distributed over the height of the braced bay; in which horizontal peak load is applied at the roof level and gradually decreased to zero at the base of the frame.

According to FEMA356 (2000) [35], the lateral load F_x applied at any floor level x shall be determined in accordance with the following two equations:

$$F_x = C_{vx} \text{ x } V \tag{4.1}$$

$$C_{vx} = \frac{w_x {h_x}^k}{\sum_{i=1}^{n} w_i {h_i}^k} \tag{4.2}$$

Herein, C_{vx} is the vertical distribution vector; k is a coefficient where k = 2 for T> 2.5s and k= 1.0 for T ≤ 2.5 s. For intermediate values, k is calculated by linear interpolation.

In addition, *V*: design base shear, w_i: building weight at the ith floor, w_x: weight of the xth floor, while h_i and h_x is the height from the base to the ith floor and xth floor, respectively.

For 3 and 9 storey storey frames the distribution of lateral loads are shown in Figure 4.2. The pushover analysis continued until the roof drift in the frame reached the drift limit of 2.5% or until non-convergence happened.

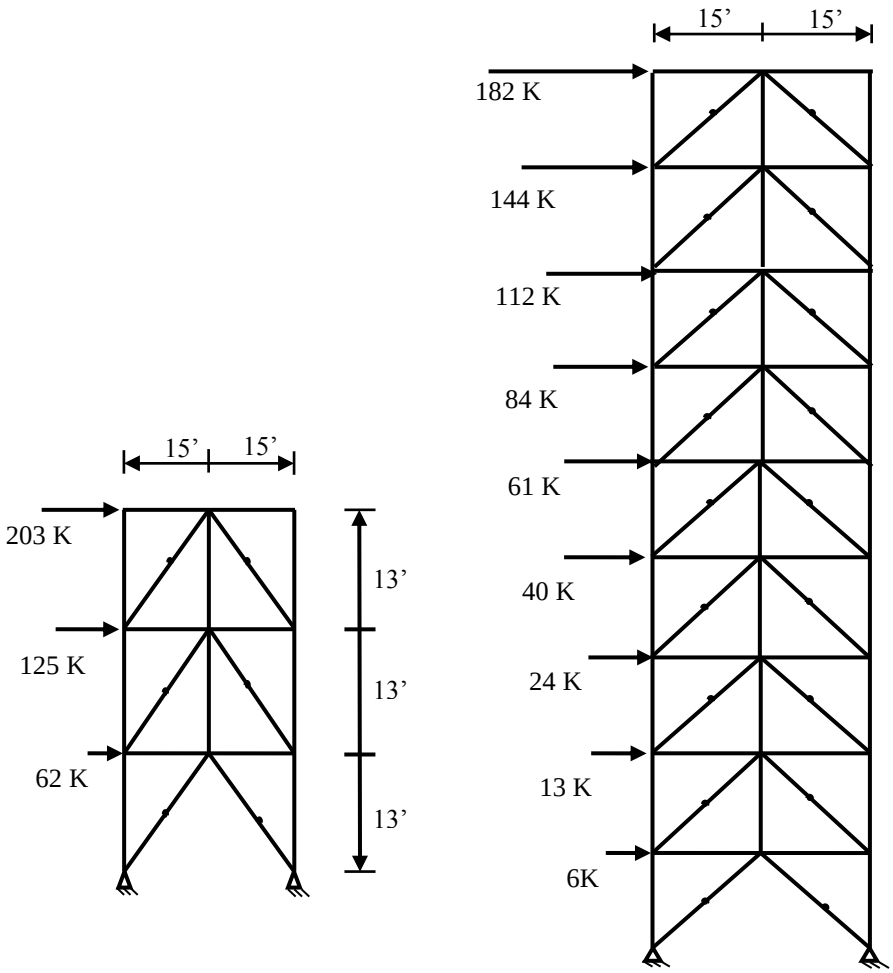

Figure 4.2: 3 and 9 storey braced bay to the lateral seismic loading [1].

4.3 Result and Discussion of Pushover Analysis

4.3.1 Pushover Curve and Inter-storey Drift

The resultant pushover curve for all three models of 3 and 9 storey frames has been shown in Figure 4.3 and 4.4.

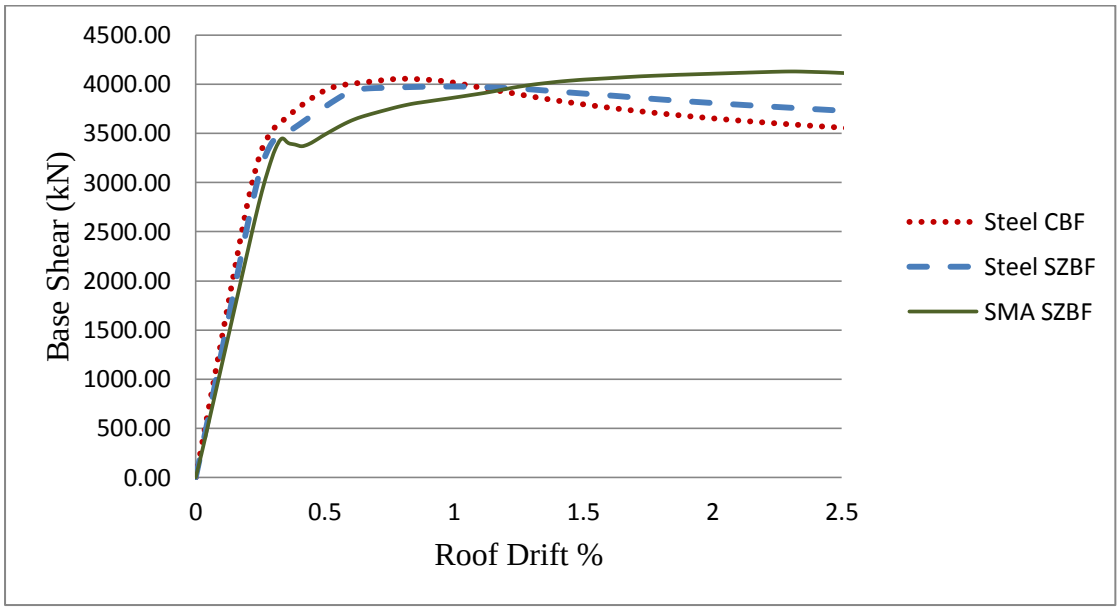

Figure 4.3: Pushover curve for 3 storey frames

From the 3 storey pushover response curves it can be observed that the lateral capacities for SMA SZBF, steel SZBF and steel CBF, are 2.38, 2.29 and 2.34 times of the design base shear and the capacity is reached at roof drift of 2.42 % and 0.76% and 0.82 % respectively.

For 9 storey frame, from pushover response curves (Figure 4.4) it can be observed that the lateral capacities for SMA SZBF, steel SZBF and steel CBF, are 1.27, 1.26 and 1.29 times of the design base shear and the capacity is reached at roof drift of 2.5%,1.67% and 0.72 % respectively. The design base shear and the results of pushover curves for 3 and 9-storey frames are also presented in Table 4.2.

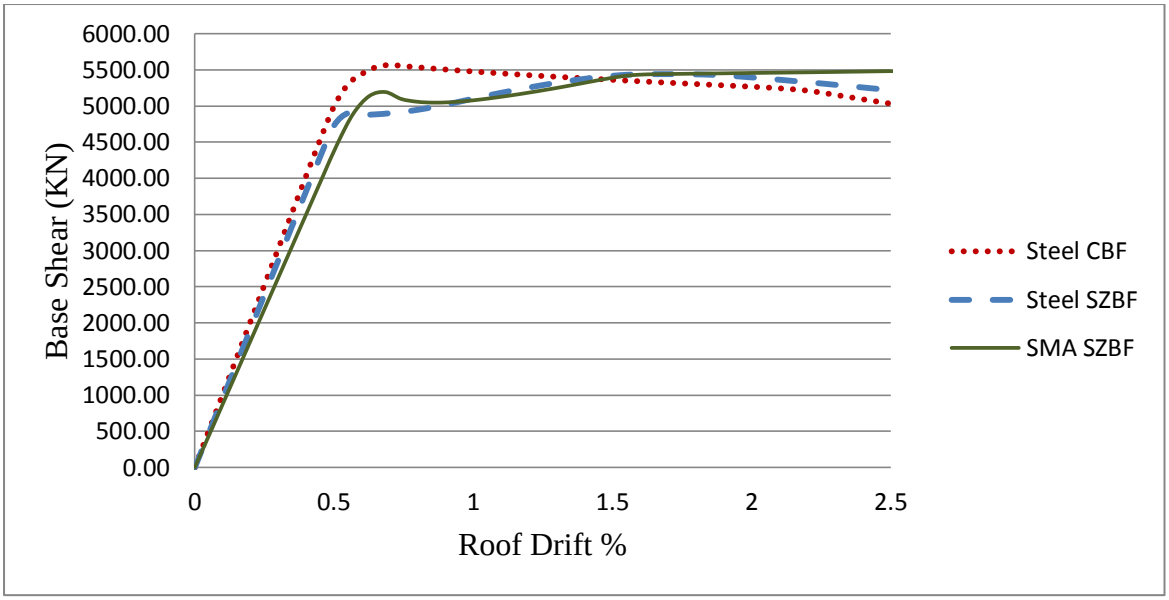

Figure 4.4: Pushover curve for 9 storey frame

The inter-storey drift distributions of the frames are depicted in Figure 4.5 (a), (b) for 3 and 9 storey frames respectively. Here the inter-storey drift represents the relative movement of the floor level either at the stage of collapse or at 2.5% maximum allowable roof drift limit.

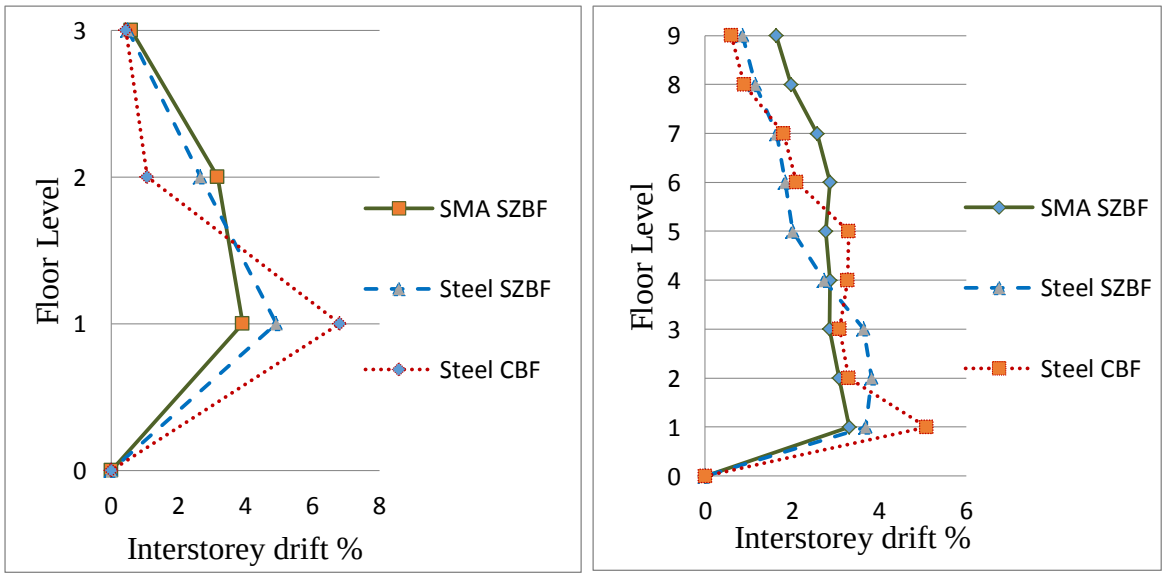

(a) (b)

Figure 4.5: Inter-storey drift % for 3 and 9 storey frame

The results from the graphs show that, the inter-storey drift ratio are more uniformly distributed in SZBF than that of CBF and within SZBF, SMA SZBF shows better results than that of steel SZBF. The maximum inter-storey drifts of 3 storey frames are 6.81%, 4.91% and 3.92% for steel CBF, steel SZBF and SMA SZBF respectively. For 9 storey frames the maximum inter-storey drifts are 5.09%, 3.68% and 3.31% for steel CBF, steel SZBF and SMA SZBF respectively.

4.3.2 Ductility and Over strength Factors

The ductility factors (R_μ) for this test structure were obtained using the equations proposed by Miranda and Bertero [37]. This method includes characteristics such as, soil conditions, ductility (μ) and natural period of the structure (T). For stiff soil:

$$R_\mu = \frac{\mu-1}{\phi} + 1 \geq 1 \qquad (4.3)$$

Where, $\phi = 1 + \frac{1}{10T-\mu T} - \frac{1}{2T}\exp[-\frac{3}{2}(\ln T - \frac{3}{5})^2]$,

μ = The displacement ductility which is defined as the ratio of the maximum displacement (Δ_{max}) to the yield displacement (Δ_y).

Over strength factor (R_o) is the ratio of the maximum base shear capacity (V_y) or actual response to the design base shear (V_d) (Figure. 4.6). Over strength factors can be calculated from the pushover curves.

$$R_o = V_y/V_d \qquad (4.4)$$

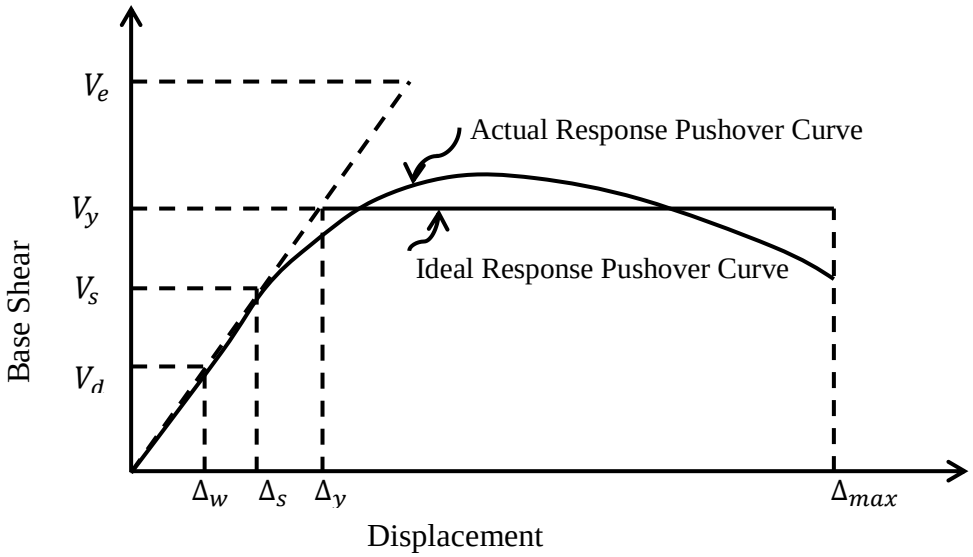

Figure 4.6: Bilinear pushover response curve to determine response modification factor

The ductility factors calculated based on the method proposed by Miranda and Bertero [37] are provided in Table 4.1. The highest ductility factor was obtained as 2.90 for 3 storey SZBFs with SMA braces. The smallest ductility factor was 2.18 for 9 storey SZBFs of SMA braces. Overall, the differences in the ductility factors of 3 storey bracings of three material configurations were large than that of the 9-storey bracings.

Table 4.1: Seismic overstrength factor and ductility of different frames.

	3 Storey			9 Storey		
	Steel SZBF	SMA SZBF	Steel CBF	Steel SZBF	SMA SZBF	Steel CBF
Design Base Shear, V_d (kN)	1736.00	1728.00	1736.00	4321.00	4321.00	4321.00
Base Shear Capacity, V_y (kN)	3977.89	4084.11	4057.43	5440.00	5501.00	5572.43
Over strength Factor, R_o	2.29	2.36	2.34	1.26	1.27	1.29
Maximum Displacement Δ_{max} (mm)	155.00	207.00	155.50	923.20	1000.00	768.90
Global Yield Displacement Δ_y (mm)	43.20	63.10	40.10	252.80	264.90	195.30
Ductility μ	3.59	3.28	3.88	3.65	3.78	3.94

4.3.3 Response Modification Factor (R)

The response modification factor R is used to reduce the linear elastic design spectrum to account for the energy dissipation capacity of the structure. It simply represents the ratio of the maximum lateral force, V_e , which would develop in a structure, responding entirely linear elastic under the specified ground motion, to the lateral force, V_d, which it has been designed to withstand. The ratio R, expressed by the equation: V_e/V_d (Figure 4.6). However, the response modification factor is determined as follows:

$$R = R_\mu . R_o \quad (4.5)$$

Where, R_μ is a reduction factor due to ductility, i.e. ductility factor and R_o is the over strength factor. The R for the SZBFs was obtained by multiplying the over strength factor with the ductility factor for each frame [10], which are listed in Table 4.2.

Table 4.2: Response modification factors

Storey		T	μ	φ	R_μ	R_o	R=$R_u . R_o$
3	Steel SZBF	0.34	3.59	1.44	2.80	2.29	6.42
	SMA SZBF	0.34	3.28	1.42	2.61	2.36	6.17
	Steel CBF	0.31	3.88	1.51	2.90	2.34	6.78
9	Steel SZBF	1.03	3.65	0.85	4.10	1.26	5.16
	SMA SZBF	1.05	3.78	0.85	4.26	1.27	5.42
	Steel CBF	1.02	3.94	0.86	4.39	1.29	5.66

The response modification factors for the frames with SMA and steel are compared in Figure 4.7. The graph shows that, The response modification factors of all 3 storey frames are above 6 and for 9 storey frames they are less than 6. So, the design consideration of R value (taking R=6 like steel CBF) of reference frames of Yang et. al. is slightly deviating

incase of 9 storey frames. However, this little deviation was not taken into consideration and designed frames of Yang's as shown in chapter 3 are continued for further proceedings of the analysis.

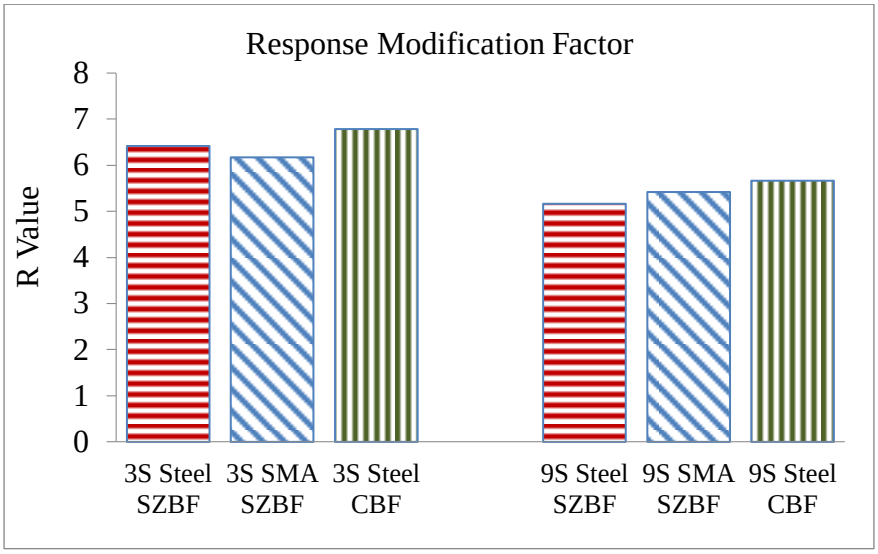

Figure 4.7: Response Modification Factor of 3 and 9 storey SZBF

4.4 Conclusion

The result of nonlinear pushover analysis indicates that, SMA SZBF exhibits excellent inter-storey drift distribution than that of steel SZBF and CBF. However, the ductility factors and response modification factors of steel braces are better than SMA braces. Moreover, lower response modification factors were obtained for frames with higher heights.

CHAPTER 5- INCREMENTAL DYNAMIC ANALYSIS OF SZBF (SMA, STEEL) AND CBF (STEEL)

5.1 Incremental Dynamic Analysis

Incremental dynamic analysis (IDA) is a parametric analysis which predicts complete structural responses and performances. The idea of IDA was first proposed by Bertero in 1977 and since then it has been developed and implemented by various researcher in their experiments. This was also adopted by the Federal Emergency Management Agency (FEMA 2000) as the state-of-the-art method to estimate the structural responses under seismic loadings. In IDA the structure is subjected to a suite of ground motion records [38], and the intensity of these ground motions are gradually increased using scale factors [39]. (E.g. peak ground acceleration is incrementally scaled from a low elastic response value up to the attainment of a pre-defined post-yield target limit state). The peak values of base shear are then plotted against their top displacement counterparts, for each of the dynamic runs, giving rise to the so-called dynamic pushover or IDA envelope curves [14]. IDA performs a huge number of non-linear time history analyses. For example, a complete IDA may have 20 or more ground motion pairs and each is scaled to 10 levels leading to 20 x 10 =200 times non-linear time history analyses. Though IDA takes a long time to perform the total analysis, it can provide the whole range of structural responses from elastic to collapse.

IDA and fragility assessment have been done to carry out the seismic analysis of the frames of this experiment. Modal analyses of all the frames were also performed to determine the fundamental periods of the frames. All mode shapes were checked to confirm the rational of the frame models and their numerical stability. IDA method was selected to analyze the buildings because it is the most accurate method to determine

building responses and to visualize the responses from elastic to inelastic then collapse. To perform IDA, a number of ground motions were selected and scaled to yield comparable IDA results for all selected ground motions. Probabilistic analysis is also essential to visualize future damage due to earthquakes. To show the probability of damage or exceedance of any limit state a fragility assessment is also performed by creating the fragility curve.

5.2 Eigen Value/ Modal Analysis

Eigenvalue or modal analyses assess the dynamic response characteristics of the frames. These analyses were performed to assure from the buildings modeling and the numerical stability, and to determine the fundamental period of the frames which was used for the selection and scaling of ground motions. SeismoStruct implements both Lanczos and Jacobi algorithms and the latter with Ritz Transformation for modal analysis [14]. In this research, the efficient Lanczos algorithm [40] was used for the evaluation of the structural natural frequencies and mode shapes. The computed periods of eigenvalue analysis of both the frames of 3 and 9 story buildings are tabulated in Table 5.1.

Table 5.1: Periods and effective modal masses percentage of SZBF and CBF.

Periods for the zipper-braced model		**1st Mode**	**2nd Mode**	**3rd Mode**
3 storey	Steel-SZBF	0.34	0.11	0.07
	SMA-SZBF	0.32	0.12	0.07
	Steel-CBF	0.31	0.12	0.07
9 storey	Steel-SZBF	1.03	0.32	0.15
	SMA-SZBF	1.05	0.36	0.15
	Steel-CBF	1.02	0.29	0.14
Factors of the effective modal masses percentages				
3 storey	Steel-SZBF	86	10	3
	SMA-SZBF	86	11	2
	Steel-CBF	84	13	2
9 storey	Steel-SZBF	76	19	4
	SMA-SZBF	75	19	5
	Steel-CBF	75	20	4

Although there is some sensitivity to higher modes, the response of the frames is essentially dominated by their first mode.

5.3 Selection of Scale Factor

In this study, the probabilistic seismic demand model (PSDM) [41] has been used to derive the analytical fragility function properties through incremental dynamic analysis of the steel frames.

Scaling approach and the cloud approach are two most common approaches for PSDM. In the scaling approach all the ground motion data are scaled to a certain specified intensity levels. On the other hand, the cloud approach uses unscaled ground motion data to perform the nonlinear time history analysis and the results obtained are used to develop the probabilistic seismic demand models. In this study, the cloud approach of PSDM has been used to determine the seismic fragility functions of the frames considered. To create sufficient data set the incremental dynamic analysis has been carried out for the cloud approach instead of nonlinear time history analysis and each ground motions data are scaled from very low peak ground acceleration to the maximum recorded peak ground acceleration for the considered ground motion. In this study, the incremental dynamic analysis was performed considering a starting scale factor of 0.10 for each ground motions data and the increment was 0.10 up to the maximum PGA for that particular ground motion. Finally, 200 time history analyses for each frame was carried out which yielded a total number of 1200 time history analysis for the six frames considered in the study. In the PSDM approach, the mean and standard deviation for different limit states were derived based on the power-law function which yields a logarithmic correlation between the engineering demand parameter and the selected intensity measure as shown below. However, data obtained from each

incremental dynamic study with scale factor 1.00 (Can be considered as Nonlinear time history analysis) has been used for determining comparative inter-storey drift and maximum roof drift ratio of all the frames considered in this analysis.

5.4 Selection of Ground Motion Records

In the nonlinear response history analysis the uncertainty characteristics associated with earthquake ground motion data largely affect the nonlinear response of the structures [4, 5]. Thereby, selection of appropriate earthquake ground motion data and the intensity measures are important steps toward analytical fragility curve development . In this study, a total of 20 ground motion data among which 10 near fault and 10 far filed were considered for the incremental dynamic analysis. Intensity measure considered for these ground motion data was the peak ground acceleration value. For this study, the near fault ground motions data were collected from the SAC steel project and the far filed earthquake ground motions data were obtained from the Applied Technology Council [34,43] far field ground motion set. All the far field ground motion data shows low to medium PGA values ranging from 0.24g to 0.73g, whereas the near fault ground motions data shows a very high PGA value ranging from 0.42g to 1.07g. The near fault and far field ground motions data were primarily categorized based on the range of epicentral distance. The epicentral distance was found to be less than 10 km for the near fault ground motions data, and epicentral distance for the far filed ground motions data were more than 10 km [4]. Only one horizontal component in the parallel direction of the building frame having higher PGA value was considered for this study. Table 5.2 and Table 5.3 present different characteristics of the earthquake ground motions data for both the near fault and far field earthquake motions considered in this study.

Table 5.2 Characteristics of near fault ground motion

EQ No	Earthquake		Recording Station	Epicentral	PGA_{max} (g)	PGV_{max} (cm/s.)
	M	Name				
NF1	7.4	Tabas	-	1.2	0.90	108
NF2	7.4	Tabas	-	1.2	0.96	103.8
NF3	7	Loma Prieta	Los Gatos	3.5	0.70	170
NF4	7	Loma Prieta	Lex. Dam	6.3	0.37	67.34
NF5	6.7	Erzincan	Erzincan	2	0.42	117
NF6	7.3	Landers	Lucrene Valley Stn.	1.1	0.79	69
NF7	6.7	Nothridge	Rinaldi	7.5	0.87	171
NF8	6.7	Nothridge	Olive View	6.4	0.72	120
NF9	6.9	Kobe	JMA	3.4	1.07	157
NF10	6.9	Kobe	Takatori	4.3	0.77	170.5

Table 5.3 Characteristics of far field ground motion

EQ No	Earthquake		Recording Station	Epicentral	PGA_{max} (g)	PGV_{max} (cm/s.)
	M	Name				
FF1	6.7	Northridge	Beverly Hills	13.3	0.42	58.95
FF2	7.3	Landers	Yermo Fire	86	0.24	52
FF3	7.3	Landers	Coolwater	82.1	0.28	26
FF4	7.1	Duzce Bolu	Bolu	41.3	0.73	56.44
FF5	6.9	Loma Prieta	Gilroy Array #3	31.4	0.56	36
FF6	6.5	ImpValley	El Centro Array#1	29.4	0.36	34.44
FF7	6.9	Kobe	Akashi	18.7	0.51	37.28
FF8	6.5	Super Hills	Poe Road	11.2	0.45	36
FF9	7.6	Chi-Chi	CHY	32	0.35	71
FF10	7.6	Chi-Chi	TCU	77.5	0.47	37

All these ground motions data were then matched with the design response spectrum of Los Angeles Area [1]. Figure 5.1, shows unscaled selected ground motions with the design response spectrum.

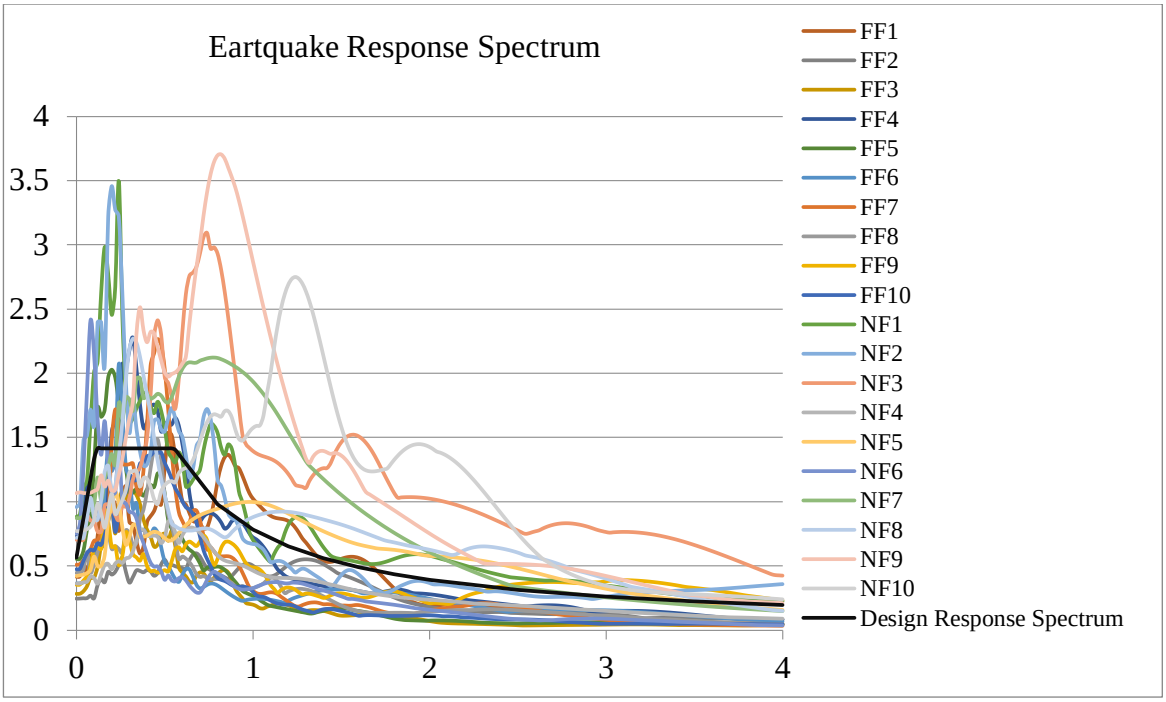

Figure 5.1 Response spectrum for the original selected ground motion pairs and the design response spectrum.

5.5 Results and Discussions of Incremental Dynamic Analysis

In this study, a total of 1200 nonlinear time history analyses were conducted on the 3 and 9 storey with 3 different bracing configurations (with the variation of materials and type). With the obtained data, the performances of different bracing configuration (steel SZBF, SMA SZBF and steel CBF) were evaluated in terms of fragility curves developed based on the probabilistic seismic demand models.

5.5.1 Dynamic Pushover Curve: Roof Drift Ratio

A dynamic pushover curve is defined as a graphical expression between maximum lateral roof displacement and corresponding base shear generated from the IDA, which provides a

continuous picture of the structural response. This curve can be used to determine structural capacity under earthquake loading [42].

Dynamic pushover curves can be generated for the frames under any specific earthquake loading. For example Figure 5.2 shows dynamic pushover curve of 3 storey SMA SZBF under GM record FF1.

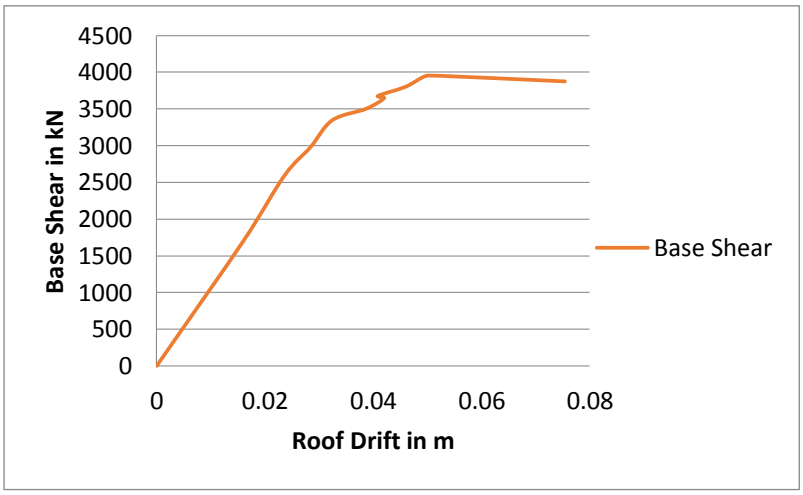

Figure 5.2: Dynamic pushover curve under GM record FF1

The demand parameters obtained from the incremental dynamic analysis are presented as dynamic pushover curves in Figure 5.3 (a) and (b). The maximum roof drift ratio was plotted against the peak ground acceleration values. All these curve shows initial linear portion before the commencement of the nonlinear portion. Investigation reveals that the steel frames has higher stiffness in the elastic region as compared SMA frames. Some dissimilarity among the IDA curves were found in the inelastic range showing softening and weaving behavior due to excessive hardening and softening of all the frames considered.

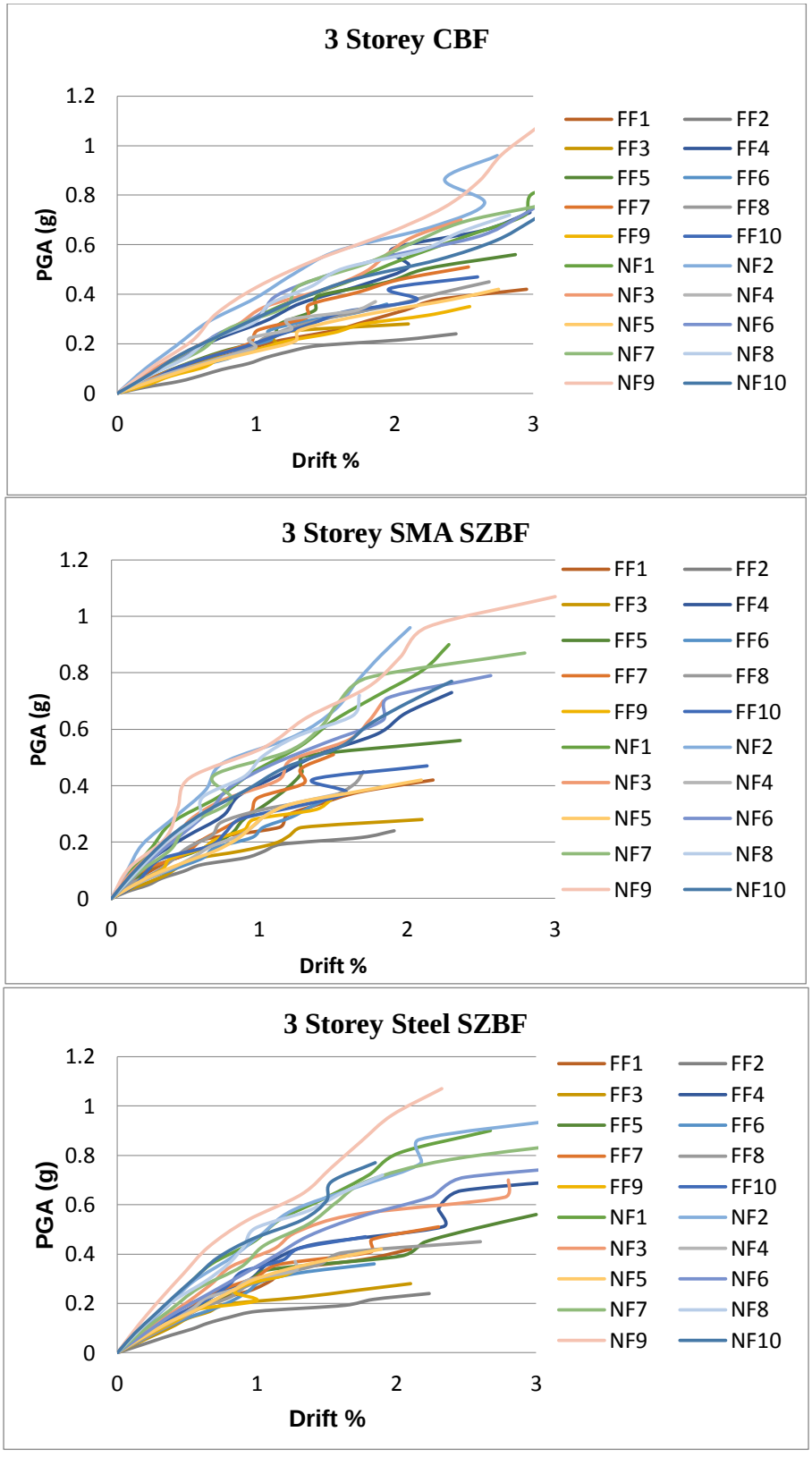

Figure 5.3 (a): IDA curve for 3 storey frames

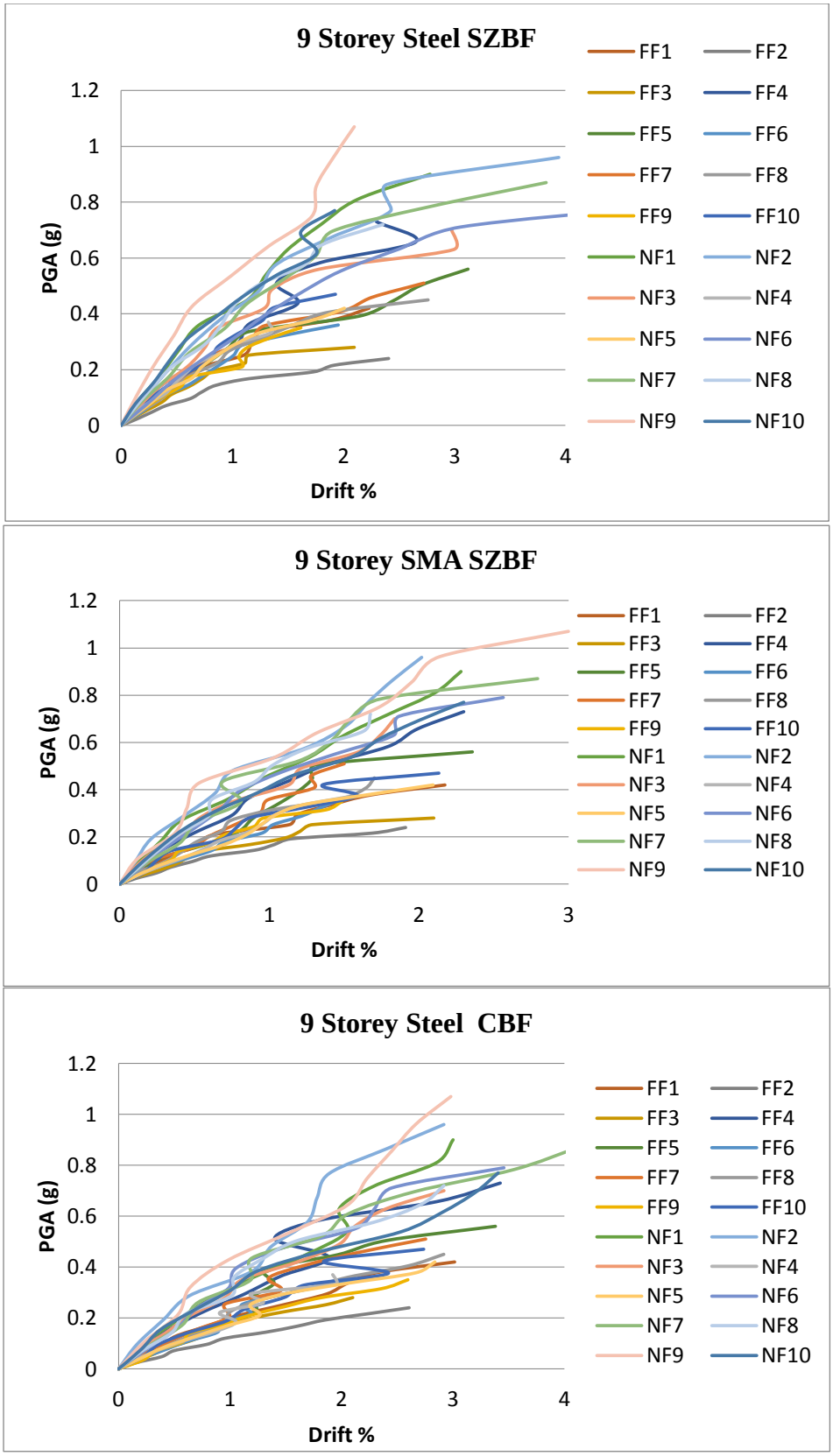

Figure 5.3 (b): IDA curve for 9 storey frames

5.5.2 Overall Response: Maximum Inter-storey Drift Ratio

The inter-storey drift percentage was computed as the difference in the displacement of two immediate floor level divided by the height of the floor [12]. An illustration of the scatter of the inter story drift demands for different earthquake ground motions are provided in Figure 5.4 (a, b). The graphs show the 16^{th}, median and 84^{th} percentile drift demands together with individual data points for the 3 story and 9 storey frames. The values of the 16^{th}, median and 84^{th} percentile employed here to represent the statistical values of the peak inter story drift ratios defined as in FEMA 355C [52]. The median of the graphs for SMA SZBF shows a uniform distribution of inter story drifts over the height than that of steel SZBF and CBF. The 16^{th} and 84^{th} percentiles also show similar patterns. For steel CBF, maximum inter-storey drift was concentrated at the first floor level showing soft/weak storey mechanism.

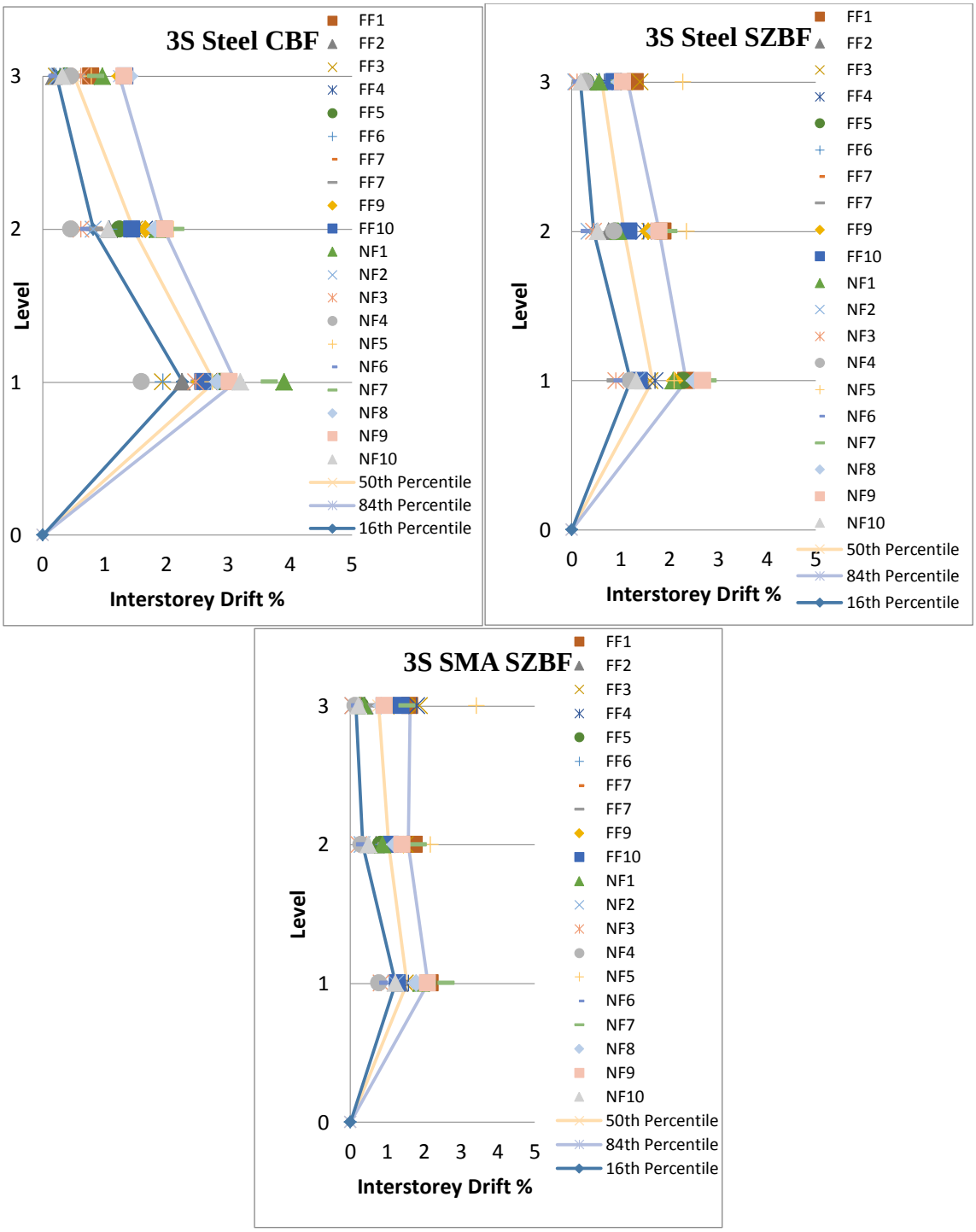

Figure 5.4 (a): Inter-storey drift profiles of 3 storey frames for far field and near fault ground motion and their 50th, 84th,16th percentile values

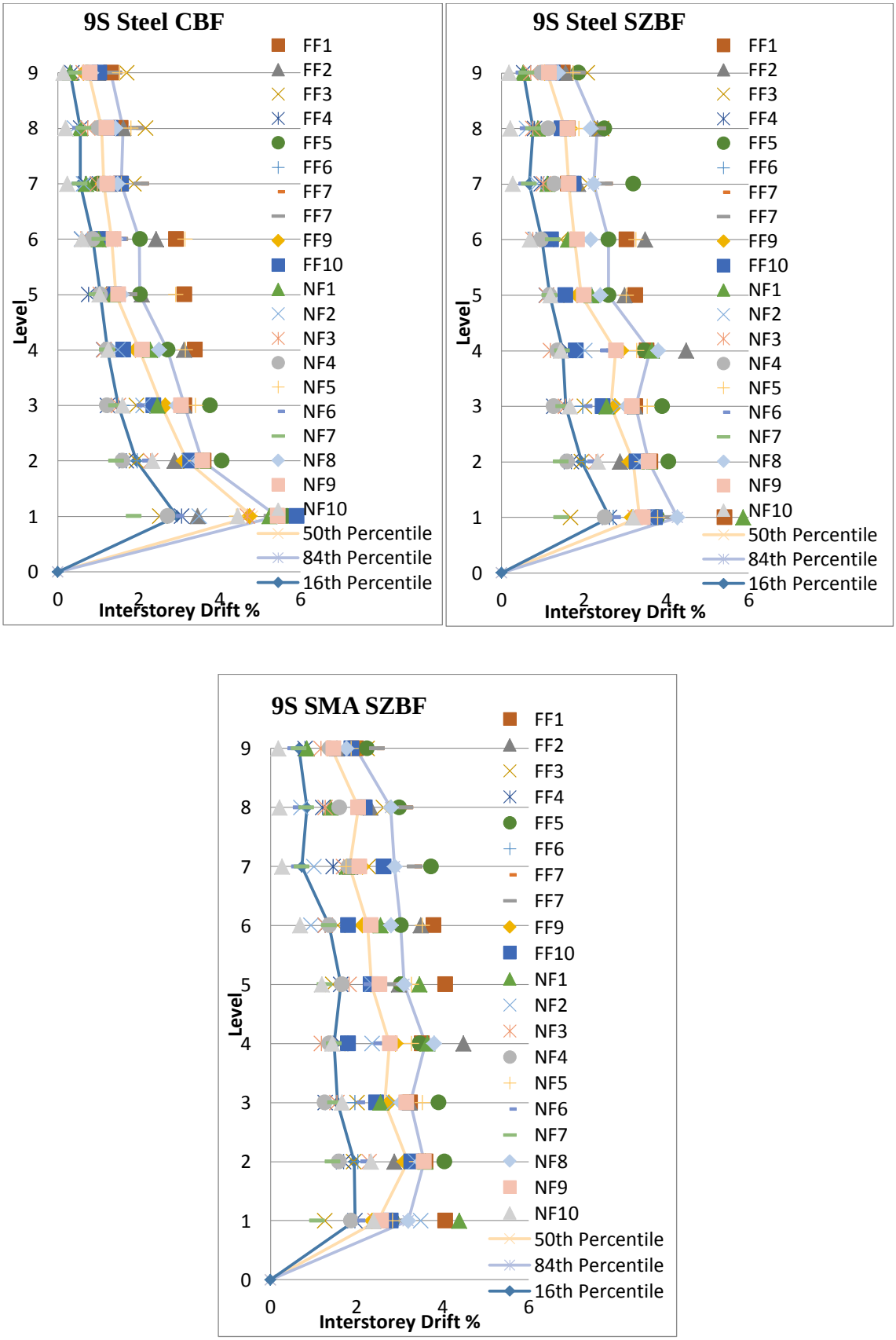

Figure 5.4 (b): Inter-storey drift profiles of 9 storey frames for far field and near fault ground motion and their 50th, 84th,16th percentile values

5.6 Probabilistic Seismic Fragility Assessment

5.6.1 Analytical Fragility Function Methodology

In the last two decades, probabilistic seismic risk assessments have been used number of times for Probabilistic Safety Analysis (PSA) of critical structures.

Probabilistic assessment is necessary for seismic response analysis because of its uncertainties especially ground motion uncertainty. In this study, fragility assessment, one of the probabilistic method, was adopted by creating fragility curves to show seismic performance of suspended zipper braced frame buildings.

5.6.2 Fragility Curve

Fragility curves is a statistical tool which shows the conditional probability of exceeding a given damage state (or performance) as a function of an engineering demand parameter (EDP) in order to evaluate seismic vulnerability of the structure. Fragility curve represents the probability of damage state of a structure as a function of ground motion intensity measure (IM). IM can be Peak Ground Acceleration (PGA), spectral acceleration at the fundamental building period with 5% damping Sa (T1 ,5%) or any other intensity measures. Figure 2.14 shows an example of a fragility curve and it can be expressed as:

$$f_{DS}(IM) = P(DS \mid IM) \tag{5.1}$$

Where,

IM = Ground motion intensity measure.

DS = Damage state.

P = Probability of exceeding a damage level.

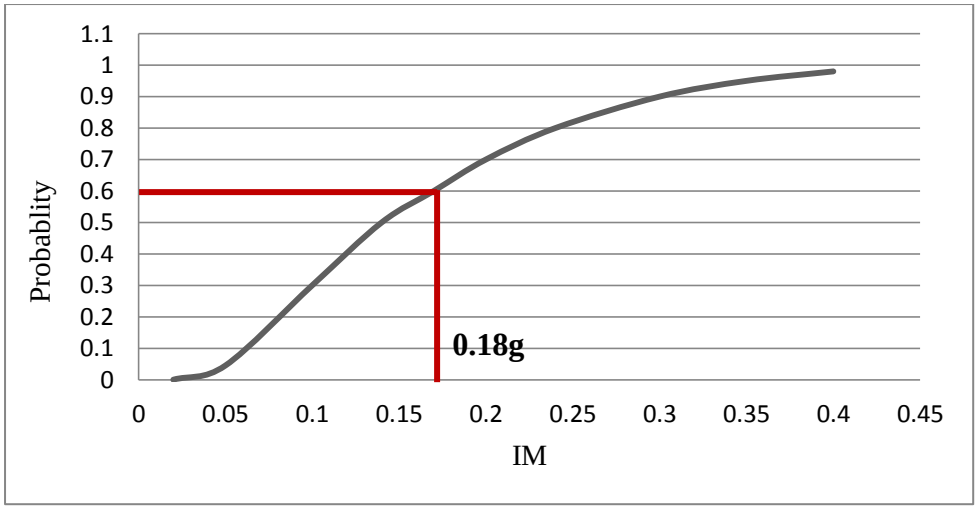

Figure 5.5: Fragility curve of collapse limit state shows the way determining the probability of 60% of collapse

Figure 5.5 shows the probability of damage state (let collapse) and the probability from 0% to 100% of collapse can be determined from the curve. For example, to determine 60% probability of collapse, determine the point on the fragility curve which has a vertical axis value equal to 0.6. Then, the value on the horizontal axis representing the ground motion intensity (i.e. IM = 0.18g) is determined which corresponds to the probability of 60% of collapse.

Methodologies developed to show fragility relationship between IM and the building responses can be classified into four types [28] which are:

- Expert based or experiential fragility curves,
- Analytical fragility curves,
- Empirical fragility curves, and
- Hybrid fragility curves.

5.6.3 Probabilistic Seismic Demand Model (PSDM)

Probabilistic seismic demand model (PSDM) is used to derive the analytical fragility function properties through incremental dynamic analysis of the building frames. The two most common approaches for PSDM are the scaling approach and the cloud approach [43]. In the scaling approach all the ground motion data are scaled to a certain specified intensity levels. In contrary, the cloud approach uses unscaled ground motion data to perform the nonlinear time history analysis and the results obtained are used to develop the probabilistic seismic demand models. For this study, the cloud approach of PSDM has been used to determine the seismic fragility functions of the frames considered. To create sufficient data set the incremental dynamic analysis has been carried out for the cloud approach instead of nonlinear time history analysis and each ground motions data are scaled from very low peak ground acceleration to the maximum recorded peak ground acceleration for the considered ground motion. In the PSDM approach, the mean and standard deviation for different limit states were derived based on the power-law function which yields a logarithmic correlation between the engineering demand parameter and the selected intensity measure as shown below:

$$EDP = a(IM)^b \tag{5.2}$$

$$ln\,(EDP) = ln(a) + b\,ln(IM) \tag{5.3}$$

Here, a and b = unknown coefficients that can be estimated through linear regression analysis of the response data collected from the incremental dynamic analysis.

The dispersion value for the demands $\beta_{EDP/IM}$ was estimated according to the equation below:

$$\beta_{EDP/IM} = SQRT \sum_{i=1}^{N} [ln\,(EDP) - \ln(aIM)^{b}]^{2} / (N-2) \quad (5.4)$$

Where, N is the total number of simulation cases. With the probabilistic seismic demand models and the limit state values for different damage state considered for this study, it is now possible to generate the seismic fragilities for the considered intensity measure and demand parameters following equation 5.

$$P\,(LS \mid IM) = \Phi \ln(IM) - \ln(IM_{n)} / \ \beta_{comp} \quad (5.5)$$

Here, Φ = standard normal cumulative distribution function and the median value of the intensity measure, IM_n was calculated using the following equation.

$$\ln(IM_{n)} = [\ln(S_{c)} - \ln(a)]/b \quad (5.6)$$

Here, S_c and β_c are the median and dispersion values for the damage states of the reinforced concrete buildings respectively. Finally, the dispersion component was calculated using equation below:

$$\beta_{comp} = SQRT[(\ \beta_{EDP/IM} + \ \beta_c{}^{2})/b \quad (5.7)$$

5.6.4 Intensity Measure and Demand Parameters

Selection of an appropriate IM is the most important step for developing seismic fragility curves. IM represents the severity of the earthquake ground motion and has been a point of research interest among the earthquake engineers. Several alternatives for intensity measure includes the first mode spectral acceleration, peak ground acceleration (PGA), peak ground velocity (PGV), peak ground displacement, spectral displacement at the fundamental time period, time duration of strong motion, spectrum intensity etc. and so on as proposed by previous researchers [44-47]. However, the spectral acceleration at the first mode of vibration (Sa, T1) or simply Sa is the

mostly commonly used IM for fragility assessment. The study of Mackie and Stojadinovic concluded that the first mode spectral acceleration and spectral displacement are the two ideal intensity measure in terms of efficiency, effectiveness and robustness [46]. On the other hand, the optimum intensity measure for the ground motion was described as the PGA value by Padgett and DesRoches [47]. Moreover, Billah et. al., investigated the suitability of five different intensity measures i.e. peak ground acceleration, peak ground velocity, peak ground displacement, spectral acceleration at 0.1s time period and spectral acceleration at 1s time period in order to determine the most efficient, practical and proficient intensity measure for fragility assessment of retrofitted bridge bents [48].

Result shows that, PGA is the most efficient and proficient intensity measure to predict the uncertainty of both the far field and near fault ground motion data. In this study, the peak ground acceleration value alone was considered as the intensity measure for the seismic fragility assessment of the retrofitted frame sections [43].

The different damage levels of the structure sustained as a result of different intensity earthquake ground motion are incorporated in the fragility assessment in terms of engineering demand parameter (EDP). Defining a suitable demand parameter and hence the different damage state is another important step for fragility curve development procedure. Roof drift ratio, maximum inter-storey drift ratio, residual roof drift ratio and the maximum residual inter-storey roof drift ratio are few common engineering demand parameters used for the fragility assessment of building structures. Different damage states of the building are then presented in terms of different EDP values. For this study, the maximum roof drift ratio was considered as the engineering demand parameter.

5.7 Analysis Output: Fragility Curve

To develop the fragility curve , a linear regression analysis of the logarithmic values of demand parameter and intensity measure was carried out to estimate the different PSDM parameters i.e. a, b and β_{EDP} /IM [49,50]. Figure 5.5 shows the probabilistic seismic demand models for the six different frames considered for this study. The regression parameters along with the dispersion values obtained from the regression analysis are presented in Table 5.4.

Table 5.4: Probabilistic seismic demand models for different frame considered

Frame Type		a	b	$\beta_{EDP/IM}$
3 storey	Steel CBF	3.5772	1.0231	0.4198
	Steel SZBF	2.7464	1.0932	0.4497
	SMA SZBF	2.7109	1.0684	0.4523
9 storey	Steel CBF	4.0124	1.0394	0.4853
	Steel SZBF	2.2423	0.9824	0.4428
	SMA SZBF	1.9748	0.7341	0.4625

It can be observed from the tabulated data that both 3 and 9 storey CBF frame has the highest dispersion in the demand (β_{EDP} /IM), whereas the least dispersion value was obtained from the SMA frames. A similar trend was observed for the median value of the demands, where CBF has the maximum median as compared to other frames. On the other hand, SMA has the lowest median value of the demands placed by the near-fault and far-filed ground motions. Result shows that, SZBF, particularly use of SMA in SZBF can significantly reduce the demand which is maximum inter-storey drift for the current study.

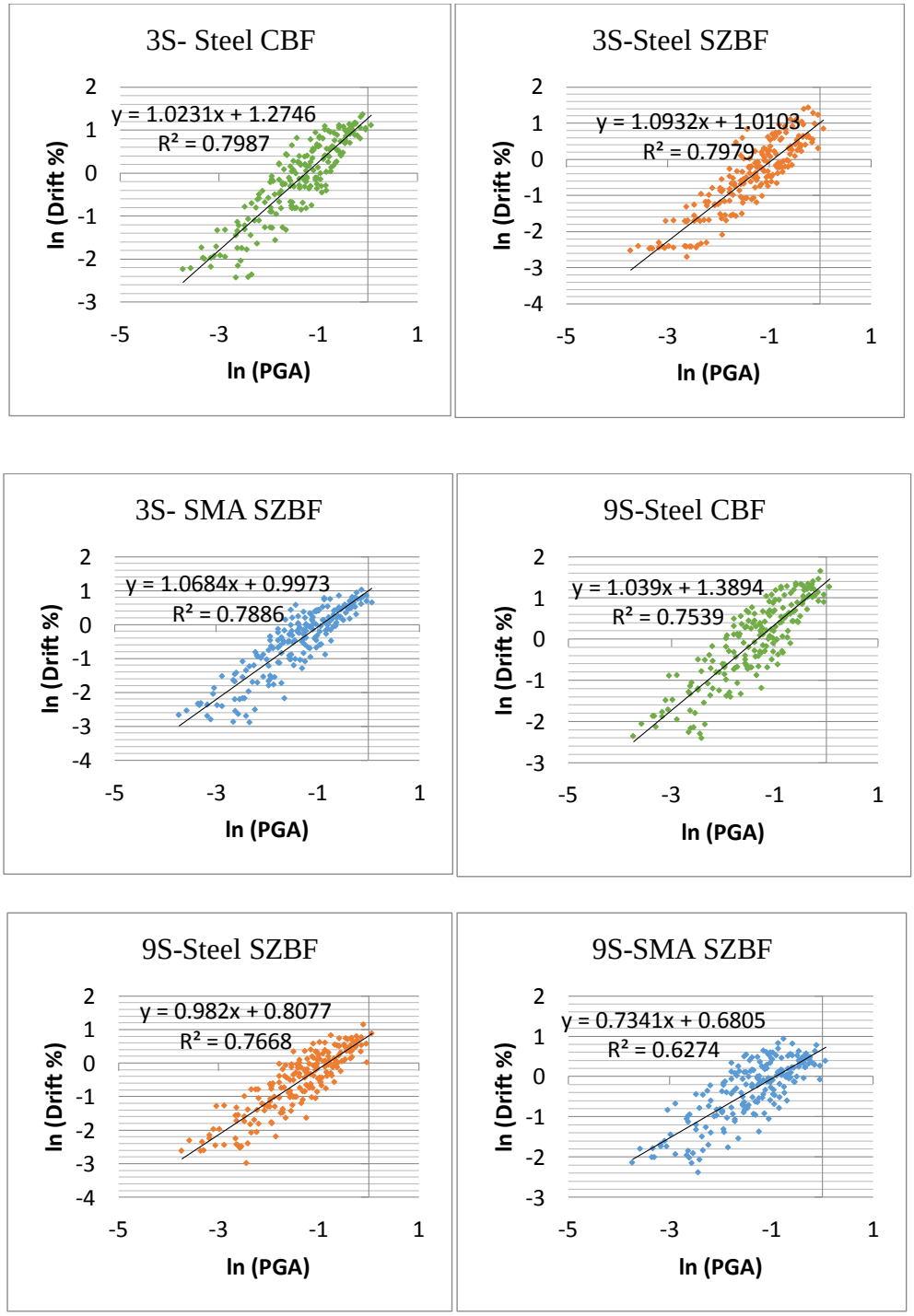

Figure 5.6 : Comparison of the PSDM for 3 and 9 storey frames.

Finally from the obtains data, fragility curves for all the six frames were developed and are presented in Figure 5.6. For this structural performance level or damage state has been considered according to guidelines of FEMA 356 [36], i.e for steel braced frame

2% drift for collapse prevention, 1.5% for life safety and 0.5% for immediate occupancy [36].

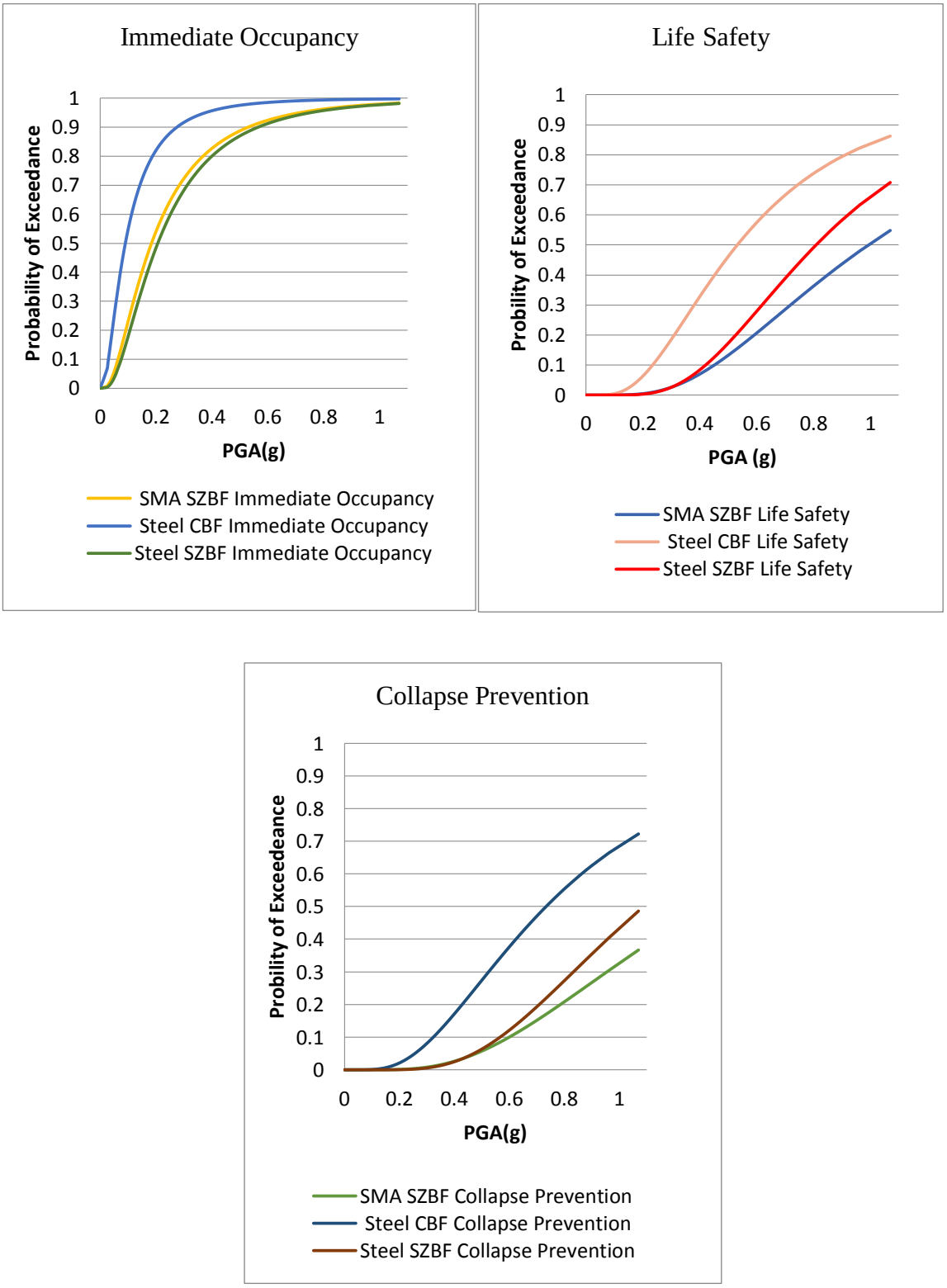

Figure 5.7 (a): Fragility curves for various damage states of 3 storey frames

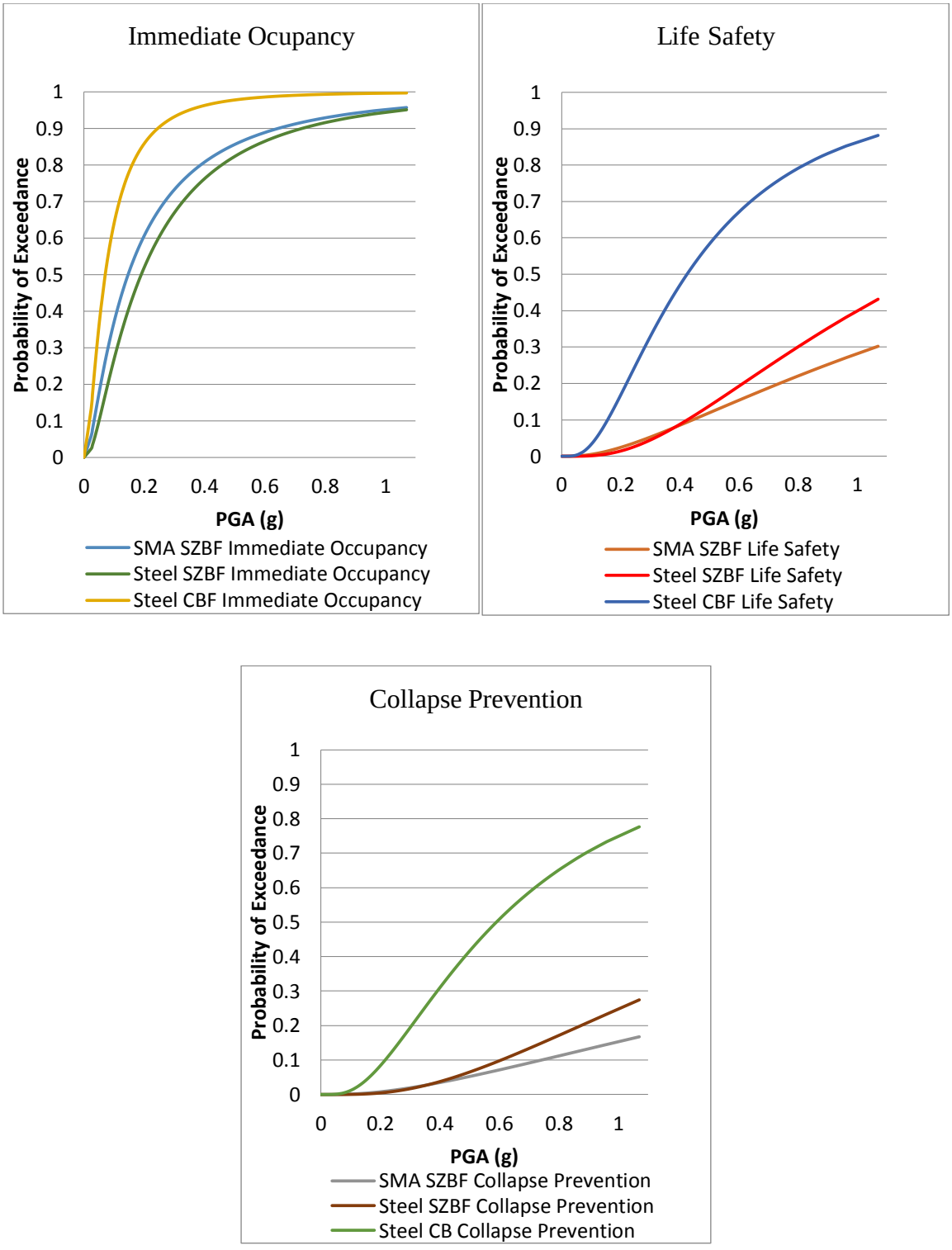

Figure 5.7(b): Fragility curves for various damage states of 9 storey frames

The probabilistic method of seismic performance evaluation offers an insightful and effective comparison method for the various frames considered in this study. The fragility parameters can be estimated from the limit state values of different damages as well as the

regression parameters obtained from the regression analysis of probabilistic seismic demand models. These curves offer the comparison and hence prediction of the effectiveness of use of SMA in SZBF.

From Figure 5.7, it is observed that the curves are very close for steel and SMA based SZBF for the case of immediate occupancy damage state. However, there is significant difference in case of CBF and SZBF which indicates that the SZBF has got the added advantage to reduce the vulnerability of damage due to excessive inter-storey drift than that of CBF. Similar trend also has been found for life safety and collapse prevention damage states. Moreover, the fragility curves for SMA SZBF frames show a slight better performance than steel SZBF in these two cases. For all the damage states, the SMA SZBF was found to be the most effective bracing system to reduce inter-storey damage vulnerability. In order to compare the effect of all these frames, an arbitrary earthquake ground motion data with peak ground acceleration value of 0.6 g was considered and the corresponding probability of exceedance of different damage states are presented in Figure 5.8.

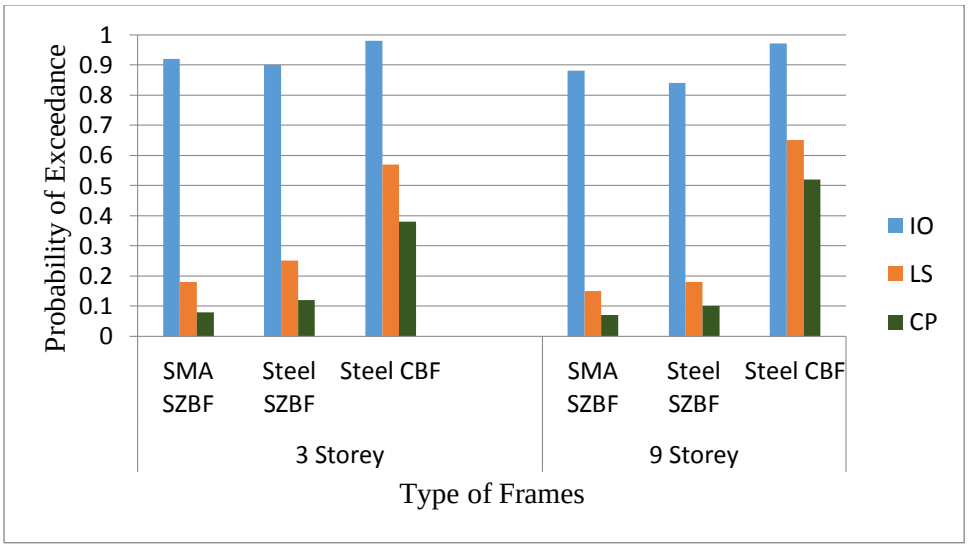

Figure 5.8: Probability of exceedance corresponding to different damage states for an arbitrary ground motion with PGA Value 0.6g

5.8 Conclusion

In this chapter, The PSDM has been used to derive the analytical fragility function properties through IDA. From the nonlinear response history analysis associated with twenty different earthquake ground motion data it is derived that, both SMA and steel SZBF show better trend with more uniform inter-storey drift ratio than that of CBF. Within steel and SMA SZBF, SMA SZBF exhibited significant improvement in terms of maximum inter-storey drift distribution over the height of the building, hence reduce the vulnerability of damage due to the excessive inter-storey drift.

CHAPTER 6- CONCLUSIONS AND RECOMMENDATION

6.1 Conclusions

6.1.1 The main outcome of this study is that SZBF structural configuration can reduce the chances of forming the weak storey mechanism and achieve a closer inter-storey drift distribution over its height than that of CBF and lessen the vulnerability of damage due to earthquake. Moreover, use of SMA brace instead of steel brace in SZBF attains better inter-storey drift distribution and can be a choice for designers in case of designing a critical structure build to sustain heavy earthquake loads.

6.1.2 Prior to going into the analysis a detail understanding of theoretical background of performance based seismic engineering is required. Thereby an effort was taken to discuss in details about the performance based seismic engineering that uses pushover analysis and incremental dynamic analysis tools to derive the output in fragility curves.

6.1.3 This paper conducted an extensive comparative study of the seismic performance of 3 and 9 storey SMA and steel SZBF and steel CBF. The result from nonlinear pushover analysis shows:

- SMA SZBF gets the peak base shear capacity beyond 2.42 % and 2.5% roof drift for 3 and 9 storey with an upward curve while other frames base shear capacity get downward curves in this drift ratio. The peak base shear capacity reached at 0.76% and 1.67% of roof drift for 3 and 9 storey SZBF, and 0.82 % and 0.72 % roof drift for 3 and 9 storey CBF respectively.
- Both 3 and 9 storey SMA and steel SZBF show better inter-storey drift distributions than that of steel CBF. In case of 9 storey frames, SMA SZBF

exhibits an appreciable distribution of inter-storey drift ratio over the height of the building.

- Response modification factor of all the frames are almost similar. However, response modification factor of 9 storey frames are less than that of 3 storey frames.

6.1.4 In this analysis, IDA was performed on each reference frame under 20 different ground motions (10 near faults and 10 far fields). The results of the analyses are:

- Steel braced frame has got higher stiffness in elastic region than that of SMA frames.
- The 50^{th}, 84^{th} and 16^{th} percentile of inter-storey drift ratio, obtained from the IDA, show that for CBF frame it is much higher in the first floor, where as, for steel SZBF they are well distributed to the upper floors. For SMA braced frames inter-storey drifts are distributed more uniformly even at the upper floors of 9 storey frames.
- The fragility curves show that probability of exceedance of all types of damage states of CBF are greater than that of SZBF. However, there is no significant difference in immediate occupancy for steel SZBF and SMA SZBF frames. But, for the damage states of life safety and collapse prevention SMA SZBF shows better performance than that of steel SZBF, specially at higher PGA values.

6.2 Recommendation for Future Research

More works can be done in future to improve the understanding of seismic performance of SMA SZBF frames as listed below:

- Experimental study can be done by a reduced-scale SMA SZBF designed in compliance with the capacity design procedure described in chapter 3 [1,15] to understand the real time strength and ductility of SMA in bracing system.
- Analytical study can be done for taller frames (12, 15, 20 storey frames etc) to visualize the effects of SMA used in zipper bracing systems of tall structure.
- SMA can be integrated only for lower stories of the tall building's frame and can be compared with full height use of SMA in the bracing systems.

References

[1] Yang C.S. (2006). Analytical and experimental study of concentrically braced frames with zipper struts. PhD Thesis, Georgia Institute of Technology.

[2] Yang C.S., Leon R.T., Des Roches R. (2007) Design and behavior of zipper-braced frames. Atlanta: School of Civil and Env. Engineering, Georgia Tech; [GA 30332–0355].

[3] Chen Z. (2012).Seismic response of high-rise zipper braced frame structures with outrigger trusses. M.Sc Thesis, Concordia University.

[4] Khatib I.F, Mahin SA, Pister KS, (1988).Seismic behavior of concentrically braced steel frames. Report No.UCB/EERC-88/01. Berkeley: Earthquake Engineering Research Center, University of California.

[5] Goel SC. (1992). Earthquake Resistant Design of Ductile Braced Steel Structures. Stability and Ductility of Steel Structures Under Cyclic Loading. Boca Raton, FL: CRC Press,p. 298–308.

[6] Bruneau M, Uang CM, Whittaker A. (1998). Ductile Design of Steel Structures. McGraw-Hill.

[7] AISC341-10 (2009). Seismic Provisions for Structural Steel Buildings. Chicago: American Institute of Steel Construction.

[8] Yang C.S, Leon RT, Des Roches R. (2008). Pushover Test and Analysis of a Braced Frame With Suspended Zipper Struts. ASCE J Struct Eng.

[9] Alam, M.S., Youssef, M.A., Nehdi, M. (2007). Utilizing shape memory alloys to enhance the performance and safety of civil infrastructure: a review. Canadian Journal of Civil Engineering; 34(9): 1075-1086.

[10] Alam, M.S., Moni, M., Tesfamariam, S. (2012).Seismic overstrength and ductility of concrete buildings reinforced with superelastic shape memory alloy rebar. Engineering Structures; 34: 8-20.

[11] Auricchio, F., Fugazza, D. and DesRoches, R. (2006). Earthquake performance of steel frames with Nitinol braces. Journal of Earthquake Engineering; 10(Sp. Issue 1):45-66.

[12] Asgarian, B. and Moradi, S. (2011) Seismic response of steel braced frames with shape memory alloy braces. Journal of Constructional Steel Research; 67: 65-74.

[13] McCormick, J., DesRoches, R., Fugazza, D. and Auricchio, F. (2007). Seismic assessment of concentrically braced steel frames with shape memory alloy braces. Journal of Structural Engineering ; 133(6): 862-870.

[14] SeismoSoft (2016). SeismoStruct - A computer program for static and dynamic nonlinear analysis of framed structured, available from http://www.seismosoft.com.

[15] Ozceilik, Y., Saritas, A., Clayton P.M. (2016) Comparison of chevron and suspended zipper braced frames. Journal of Constructional Steel Research; 119: 169-175.

[16] Chen, L. (2011). Master Thesis: Innovative brace system for earthquake resistant concentrically braced frame structures. Montreal: Department of Building, Civil & Environmental Engineering, Concordia University.

[17] Sabelli, R., (2001). Research on improving the design and analysis of earthquake-resistant steel-braced frames. NEHRP fellowship report No.PF2000-9, Earthquake Engineering Research Institute, Oakland, CA.

[18] Tremblay, R., and Trica, L. (2003).Behavior and design of multi-story zipper concentrically braced steel frames for the mitigation of soft-story response, Proceedings of the STESSA Conference on Behavior of Steel Structures in Seismic Areas, Naples, Italy.

[19] Bruneau, M., Engelhardt, M., Filiatrault, A., Goel, S. C., Itani, A., Hajjar, J., Uang, C. M. (2005). Review of selected recent research on US seismic design and retrofit strategies for steel structures. Progress in Structural Engineering and Materials, 7(3), 103-114.

[20] Leon, R., and Yang, C. (2003). Special inverted-v-braced frames with suspended zipper struts. International workshop on steel and concrete composite construction, pp. 89-96. Taipei (Taiwan) National Center for Research on Earthquake..

[21] Jason M.C., DesRoches R, Fugazza D and Auricchio F. Seismic Assessment of Concentrically Braced Steel Frames with Shape Memory Alloy.

[22] Moradi S, Alam M. S and Asgarian B. (2014). Incremental dynamic analysis of steel frames equipped with NiTi shape memory alloy braces. The Structural Design of Tall and Special Buildings.

[23] Yang W, DesRoches R, Leon RT (2010). Design and analysis of braced frames with shape memory alloy and energy-absorbing hybrid devices. Engineering Structures 2010; 32:498-507.

[24] McCormick, J. and DesRoches, R. (2003), Seismic response using smart bracing elements, The Proc. of the Extreme Loading Conf., Toronto, Canada.

[25] Ozcelik, Y. Saritas, A. Clayton P., (2015). "Comparison of low-rise steel chevron and suspended zipper braced frames", 8th International Conference on Behavior of Advances in Steel Structures, Lisbon, Portugal.

[26] Filippou F.C., Popov E.P., Bertero V.V. [1983] "Effects of bond deterioration on hysteretic behaviour of reinforced concrete joints," Report EERC 83-19, Earthquake Engineering Research Center, University of California, Berkeley,1983.

[27] Filippou F.C., Fenves G.L. (2004)."Methods of analysis for earthquake-resistant structures", Chapter 6 in 'Earthquake Engineering - From Engineering Seismology to Performance-Based Engineering', eds. Y. Bozorgnia and V.V. Bertero, Cambridge University Press, Cambridge, United Kingdom,.

[28] Correia AA, Virtuoso FB (2006) Nonlinear analysis of space frames. In: Motasoares CA, Martins JAC, Rodrigues HC,. (eds) III European Conference on Computational Mechanics. Dordrecht: Springer, p. 107

[29] Menegotto M., Pinto P.E. (1973). "Method of analysis for cyclically loaded R.C. plane frames including changes in geometry and non-elastic behaviour of elements under combined normal force and bending," Symposium on the Resistance and Ultimate Deformability of Structures Acted on by Well Defined Repeated Loads, International Association for Bridge and Structural Engineering, Zurich, Switzerland, pp. 15-22..

[30] Auricchio F., Sacco E.(1997) "A superelastic shape-memory-alloy beam," Journal of Intelligent Materials and Structures, Vol. 8, pp. 489.

[31] Alam, M.S., Nehdi, M., and Youssef, M.A. (2009). Seismic performance of concrete frame structures reinforced with super elastic shape memory alloys. Smart Structures and Systems 5(5):565-585.

[32] Asgarian, B. and Moradi, S. (2011) Seismic response of steel braced frames with shape memory alloy braces. Journal of Constructional Steel Research; 67: 65-74.

[33] Akbas, B., Kara, F.I., and Tugsal, U.M. (2007), Comparison of Pushover Analysis and Nonlinear Dynamic Time History Analysis on Low-, Medium-, and High-Rise

Steel Frames, Project No. 02-A-02-01-03, Scientific Research ProjectFund, Gebze Institute of Technology

[34] Applied Technology Council, ATC-40. Seismic evaluation and retrofit of concrete Buildings, California, 1996; Vols. 1 and 2.

[35] Federal Emergency Management Agency (FEMA), (1997).NEHRP provisions for the seismic rehabilitation of buildings. Rep FEMA 273 and 274. Washington, DC: FEMA.

[36] FEMA 356. (2000). Prestandard and commentary for the seismic rehabilitation of buildings. Federal Emergency Management Agency, Washington, D.C.

[37] Miranda, E., & Bertero, V. V. (1994). Evaluation of strength reduction factors for earthquake-resistant design. Earthquake spectra, 10(2), 357-379.

[38] Vamvatsikos, D. & Cornell, C.A. (2005). Seismic performance, capacity and reliability of structures as seen through incremental dynamic analysis. John A. Stanford, California, Blume Earthquake Engineering Research Center.

[39] Haselton, C. B., Whittaker, A. S., Hortacsu, A., Baker, J. W., Bray, J., & Grant, D. N. (2012). Selecting and scaling earthquake ground motions for performing response history analyses. Proceedings of the 15th World Conference on Earthquake Engineering. Lisbon, Portugal.

[40] Hughes T.J.R. (1987) The finite element method, linear static and dynamic finite element analysis, Prentice-Hall.

[41] Cornell C.A., Jalayer F, Hamburger, R.O. Foutch, D.A. (2002), “The Probabilistic Basis for the 2000 SAC/FEMA Steel Moment Frame Guidelines.” Journal of Structural Engineering, ASCE, Vol. 128, No. 4, pp. 526-533.

[42] Elnashai AS, Sarno LD. (2008).Fundamentals of Earthquake Engineering. John Wiley & Sons: United Kingdom.

[43] Murtuz A.K.M.G (2016). Vulnerability assessment of garment factory buildings under earthquake hazard. Master's Thesis, Military Institute of Science and Technology.

[44] Giovenale, P., Ciampoli, M., & Jalayer, F. (2003). Comparison of ground motion intensity measures using the incremental dynamic analysis. In A. Der Kiureghian, S. Madanat, & J. Pestana (Eds.), Proceedings of Applications of Statistics and Probability in Civil Engineering (pp. 1483–1491). Rotterdam: Millpress.

[45] Mackie, K.R., & Stojadinovic, B. (2007). Performance-based seismic bridge design for damage and loss limits States. Earthquake Engineering and Structural Dynamics, 36, 1953–1971.

[46] Mackie, K. R., & Stojadinović, B. (2005). Fragility basis for California highway overpass bridge seismic decision making. Pacific Earthquake Engineering Research Center, College of Engineering, University of California, Berkeley.

[47] Padgett, J.E., & DesRoches, R. (2008). Methodology for the development of analytical fragility curves for retrofitted bridges. Earthquake Engineering and Structural Dynamics, 37, 157–174.

[48] Billah, A. M., Alam, M. S., & Bhuiyan, M. R. (2012). Fragility analysis of retrofitted multicolumn bridge bent subjected to near-fault and far-field ground motion. Journal of Bridge Engineering, 18(10), 992-1004.

[49] Choi, E., DesRoches, R., & Nielson, B. (2004). Seismic fragility of typical bridges in moderate seismic zones. Engineering Structures, 26(2), 187-199.

[50] Shinozuka, M., Feng, M. Q., Kim, H. K., & Kim, S. H. (2000). Nonlinear static procedure for fragility curve development. Journal of engineering mechanics, 126(12), 1287-1295.

[51] OpenSEES, the Open System for Earthquake Engineering Simulation, is an object-oriented, software framework , available from http://www. http://opensees.berkeley.edu.

[52] FEMA-355C, (2000). State of the art report on systems performance of steel moment frames subject to earthquake ground shaking, prepared by the SAC joint venture for the Federal Emergency Management Agency, Washington, DC.